

Review

A Perspective on Low-Temperature Water Electrolysis – Challenges in Alkaline and Acidic Technology

Maximilian Schalenbach^{1,*}, Aleksandar R. Zeradjanin^{1,2}, Olga Kasian¹, Serhiy Cherevko^{1,2},
Karl J.J. Mayrhofer^{1,2,3,*}

¹ Department of Interface Chemistry and Surface Engineering, Max-Planck-Institut für Eisenforschung GmbH, Max-Planck-Strasse 1, 40237 Düsseldorf, Germany

² Helmholtz-Institute Erlangen-Nürnberg for Renewable Energy (IEK-11), Forschungszentrum Jülich, Egerlandstr. 3, 91058 Erlangen, Germany

³ Department of Chemical and Biological Engineering, Friedrich-Alexander-Universität Erlangen-Nürnberg, Egerlandstr. 3, 91058 Erlangen, Germany

*E-mail: m.schalenbach@mpie.de, k.mayrhofer@fz-juelich.de

Received: 31 October 2017 / Accepted: 1 December 2017 / Published: 28 December 2017

Water electrolysis is considered as an important technology for an increased renewable energy penetration. This perspective on low-temperature water electrolysis joins the dots between the interdisciplinary fields of fundamental science describing physicochemical processes, engineering for the targeted design of cell components and the development of operation strategies. Within this aim, the mechanisms of ion conduction, gas diffusion, corrosion and electrocatalysis are reviewed and their influence on the optimum design of separators, electrocatalysts, electrodes and other cell components are discussed. Electrocatalysts for the water splitting reactions and metals for system components are critically assessed towards their stability and functionality. On the basis of the broad scientific analysis provided, challenges for the design of water electrolyzers are elucidated with special regard to the alkaline or acidic media of the electrolyte.

Keywords: Hydrogen Evolution Reaction (HER), Oxygen Evolution Reaction (OER), Hydrogen Production, Electrocatalysts, Electrolytes

TABLE OF CONTENTS:

1. INTRODUCTION

2. FUNDAMENTALS

2.1. *The reactions: Thermodynamics and kinetics*

2.2. *Cell and system design*

3. ELECTROLYTES AND SEPARATORS

3.1. *Ohmic drop and gas cross-permeation*

- 3.2. *Porous separators*
- 3.3. *Polymer electrolyte membranes*
- 3.4. *Physical properties of electrolytes*
- 3.5. *Gas evolution and bubble formation*
- 3.6. *Comparison of porous separators and SPEs*
- 3.7. *Section summary*

4. ELECTROCATALYSTS

- 4.1. *Stability*
- 4.2. *Activity descriptors*
- 4.3. *Hydrogen evolution reaction (HER)*
- 4.4. *Oxygen evolution reaction (OER)*
- 4.5. *Surface area*
- 4.6. *Composite and alloy electrocatalysts*
- 4.7. *Electrocatalysts in water electrolyzers*
- 4.8. *Section summary*

5. ELECTRODES, CURRENT COLLECTORS AND BIPOLAR PLATES

- 5.1. *Electrodes*
- 5.2. *Current collectors and bipolar plates*

6. CELL PROPERTIES

- 6.1. *Voltage-current characteristic*
- 6.2. *Heat balance*
- 6.3. *Gas purities and pressurized operation*
- 6.4. *Cell efficiency*
- 6.5. *Durability*
- 6.6. *Section summary*

7. MAJOR TECHNICAL CHALLENGES

8. SUMMARY

1. INTRODUCTION

Water electrolysis means the electrochemical decomposition of water by electric energy using two electrodes immersed in an electrolyte. After its first observation in the late 18th century, Michael Faraday first described the relation between the electric current (or charge) and the amount of evolved hydrogen and oxygen at the electrodes. Commercial alkaline water electrolysis with liquid bases as the electrolyte was already commercially used in the beginning of the 20th century. These alkaline water electrolyzers consisted of nickel electrodes and porous separator such as asbestos or cardboard in between them. In late 1960, General Electric first presented water electrolyzers with acidic solid polymer electrolytes (SPEs) [1]. Today, the electrode structure in SPE water electrolyzers is based on decades of intensive research, experience and development of SPE fuel cells and water electrolyzers. With solid perfluorated sulfonic acids as the SPEs, platinum based catalysts for the cathode and

iridium based catalysts for the anode, state-of-the-art SPE water electrolyzers still consist of the same core materials as the very early ones [2]. In the case of industrial alkaline water electrolysis, nickel as the active component for the anodic and cathodic catalyst still represents the state-of-the-art [3], while various improvements of the porous separator [4,5] and the electrode design were presented in the late 20th century [6].

In modern times, low-temperature water electrolysis displays an efficient technology to convert the electric energy supplied by renewables into chemical energy in the form of hydrogen [7,8] and is considered to represent a key technology for a renewable energy economy [9]. The hydrogen produced can be used as a manifold chemical for the combustion in heat engines [10], to generate heat, conversion to electric energy using fuel cells [11,12], methanation of carbon dioxide [13,14], production of hydrocarbons as liquid fuels or the basis of synthetic organic chemistry [15], in metallurgy processes [16,17], for ammonia synthesis [18], to name just a few.

The content of this perspective is structured as follows: First, the fundamentals of water electrolysis, the thermodynamic framework and the setup of water electrolysis cells are described. Thereafter, separator and membrane materials are reviewed, while the ionic conductivity and gas permeability of the electrolytes are considered in detail. Next, stability and activity of electrocatalysts are discussed. Thereafter, the interface of the electrolyte and electrocatalysts is considered. On the basis of this detailed analysis, the choice of materials, their design, and their influence on the cell performance are discussed. Within this scope, we tried to compile a unique overview of these interdisciplinary fields. On the basis of this detailed analysis, the major challenges for the improvement of acidic and alkaline electrolyzers are highlighted.

2. FUNDAMENTALS

2.1. Thermodynamics and kinetics

When a voltage is applied to two electrodes immersed in an aqueous electrolyte, water can be electrochemically decomposed by evolving hydrogen at the negative pole, the cathode, and oxygen at the positive pole, the anode. At the electrodes, heterogeneous electrocatalysts in the form of metals or metal oxides are typically used to speed up the electrochemical reactions. Faraday's law

$$I = z \dot{n} F \quad (1)$$

relates the mole flux \dot{n} of the produced hydrogen or oxygen to the applied current I (with respect to a current efficiency of 100%), where $F = 96485 \text{ C mol}^{-1}$ denotes the Faraday constant and z the number of electrons involved in the considered anodic or cathodic half-reaction (that are stated in Table 1).

Table 1. Anodic and cathodic reactions of water electrolysis in acidic and alkaline media.

	Acidic	Alkaline
Anode	$2\text{H}_2\text{O} \rightarrow 4\text{H}^+ + \text{O}_2 + 4\text{e}^-$	$4\text{OH}^- \rightarrow \text{O}_2 + 2\text{H}_2\text{O} + 4\text{e}^-$
Cathode	$2\text{H}^+ + 2\text{e}^- \rightarrow \text{H}_2$	$2\text{H}_2\text{O} + 2\text{e}^- \rightarrow 2\text{OH}^- + \text{H}_2$

The pH of the electrolyte determines whether mainly protons or hydroxide ions are involved in the anodic and cathodic reactions. Table 1 displays the electrochemical redox-reactions of water electrolysis in acidic and alkaline electrolytes. In order to enable high ionic conductivity between the electrodes, a high amount of the charge carriers in the form of protons or hydroxide ions must be provided, which means that either strong acids or bases are typically used as the electrolytes for technical water electrolyzers. When the same electrolyte is used at the anode and cathode, the thermodynamics of water electrolysis (which is basically determined by the difference between the anodic and cathodic equilibrium potentials) is pH independent.

Stationary conditions during water electrolysis mean constant pressure, temperature and current. In this case, Gibbs free energy ΔG (also referred to as the thermodynamic reversible energy) of the water decomposition equals the change of the chemical potentials. When liquid water is decomposed into the gaseous hydrogen and oxygen, the resulting phase transition leads to an increase of the entropy S . Gibbs free energy does not describe the energy consumption of this phase transition. In contrast, the enthalpy ΔH includes the reversible character of the reaction and the irreversible contributions in the form of latent heat. With respect to constant temperature and pressure, the Gibbs-Helmholtz relation connects Gibbs free energy, enthalpy and entropy:

$$\Delta H = \Delta G + T\Delta S \quad (2)$$

Gibbs free energy at standard conditions is often referred to as the lower heating value (LHV), while the enthalpy at standard conditions is referred to as the higher heating value (HHV). By dividing with Faraday's constant F times the amount of electrons involved in the hydrogen production, Gibbs free energy and the enthalpy of water electrolysis can be expressed as voltages:

$$U_{\text{rev}} = \frac{\Delta G}{2F} \quad (3)$$

$$U_{\text{ent}} = \frac{\Delta H}{2F} \quad (4)$$

As ΔG represents the reversible thermodynamic work, the related reversible voltage U_{rev} equals the difference of the cathodic and anodic equilibrium potentials. The enthalpic or thermoneutral voltage U_{ent} accounts for the reversible voltage plus the amount of energy for the phase transition of the liquid reactant (water) to the gaseous products (hydrogen and oxygen).

At standard conditions the voltages equal $U_{\text{rev}} = 1.23\text{V}$ and $U_{\text{ent}} = 1.48\text{V}$. Derived from Gibbs free energy, the influence of the temperature and pressure on the difference of the equilibrium electrode potentials is characterized by the Nernst voltage U_{N}

$$U_{\text{N}} = U_{\text{rev}}(T) - \frac{RT}{2F} \ln \left(\frac{p_{\text{H}_2} \sqrt{p_{\text{O}_2}}}{p_0^{3/2} a_{\text{H}_2\text{O}}} \right), \quad (5)$$

where p_{H_2} denoted the partial hydrogen pressure at the cathodic catalyst, p_{O_2} partial oxygen pressure at the anode, $p_0 \approx 1 \text{ bar}$ the standard pressure, and $a_{\text{H}_2\text{O}}$ the activity of water at the electrodes. By applying cell voltages U_{cell} of $U_{\text{N}} \leq U_{\text{cell}} < U_{\text{ent}}$, the reaction is endothermic by consuming the heat of the cell. At higher cell voltages than U_{ent} , the reaction is exothermic and thus produces heat.

Analogously to chemical reactions, the electrochemical reactions of water electrolysis are thermally activated processes in which activation energies are overcome in the form of random thermal

movement of the involved reactants and products. The Boltzmann distribution describes the reaction rate f of such processes by

$$f \propto e^{\frac{-E_A}{RT}}, \quad (6)$$

where E_A denotes the activation energy and R the gas constant. In the case of water electrolysis, the activation energy for the reactions is a function of the potential differences between the thermodynamic potentials of the reactions and the electrode potentials. Besides temperature and potential difference, the properties of the catalyst affect the activation energy. The reaction rate can be correlated to the current by Faraday's law.

The current at a catalyst for a defined overpotential is proportional to its accessible surface area. Accordingly, in order to describe the activity of a catalyst, the current is typically normalized to its surface area. On the basis of the Boltzmann distribution and Faraday's law, the Butler-Volmer relation can be derived [19], which relates the reaction rate in form of the current density to the kinetic overpotential U_{kin} of a half reaction at an electrode. The charge transfer coefficients α_c and α_a and the exchange current density j_0 parameterize this relation. In the limit of high overpotentials, one of the exponential terms in the latter equation shows negligible contributions leading to the approximation [20]:

$$|U_{\text{kin}}| \approx \frac{RT}{F \alpha z} \ln(j/j_0) \quad (7)$$

In a semi-logarithmic depiction this latter equation linearizes, from which the kinetic parameters in the form of j_0 and α are typically derived. This procedure is typically denoted as Tafel analysis.

2.2. Cell and system design

In the following, the cell design of water electrolyzers is briefly described. Detailed information on the materials and design of the separators, catalysts, and electrodes will be given from Section 3 to 5. To electrochemically decompose water, the electrodes must be connected by an ion conducting electrolyte and an electric power supply. Thus, separated pathways for the ion and electron transport between the electrodes are achieved. A separator in the form of a porous material (diaphragm) filled with a liquid electrolyte or a solid polymer electrolyte (SPE) membrane between the electrodes avoids extensive mixing of the hydrogen and oxygen evolved. In SPEs, ionizable functional groups lead to water uptake and an acidic or alkaline aqueous phase. In the case of a diaphragm, a liquid electrolyte such as an aqueous solution of KOH must be used to provide the ionic conductivity between the electrodes. Figure 1 illustrates the setup of a bipolar water electrolysis cell [21] in a zero gap configuration [4,22], in which the electrodes are in direct contact to the separator/membrane. Historical monopolar cell designs and non-zero gap configurations are not considered in this review, as these typically show low efficiency.

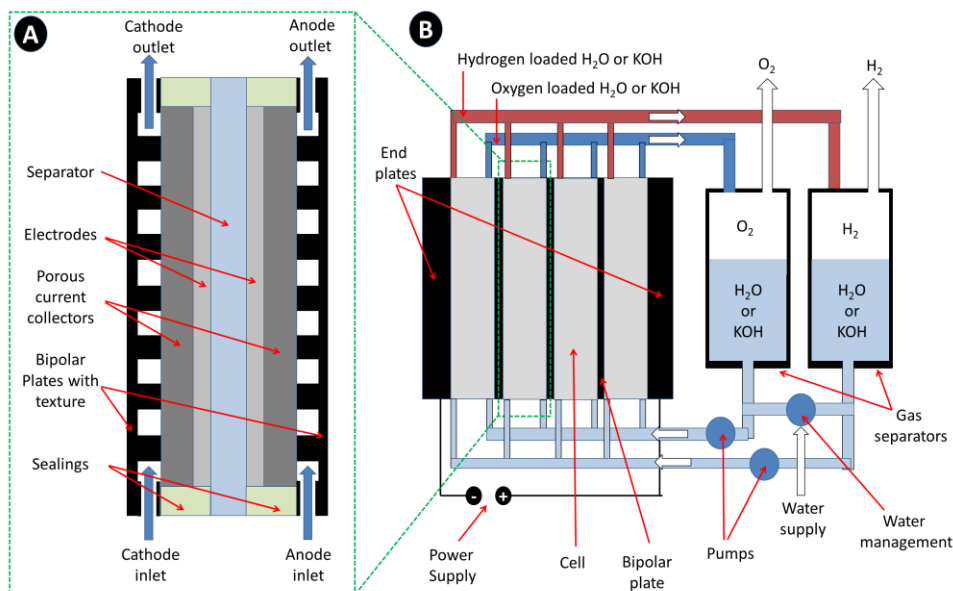


Figure 1. Schematic illustrations of a bipolar water electrolysis cell (A) and a water electrolysis system (B).

In order to enable the electrochemical reactions displayed in Table 1, electrons, ions, and water must gain access to the electrocatalysts at electrodes, while the produced gases must leave the catalysts in order to avoid their blockage by bubbles. These requirements are typically fulfilled by porous electrode structures. In the case of water electrolyzers with SPEs, the electrodes are typically realized by composites of SPE binder mixed with nanoparticle metal catalysts. In the case of water electrolyzers with liquid electrolyte, typically porous metal structures are used as electrodes. The electric current is applied to metallic end plates of the water electrolyzer. When cells are connected in series, bipolar plates separate neighboring cells. This configuration is commonly referred to as ‘stack’ of electrolysis cells.

Using SPEs for water electrolysis means that only the components that are in direct contact to the SPE are exposed to its corrosive alkaline or acidic pH, as the Coulombic force captures the hydroxide ions or protons inside the SPE (as further discussed in Section 3). Accordingly, when SPEs are used, pure water can be supplied to the electrolysis cell, which means that tubing and bipolar plates of the electrolyzer can be realized by cheap materials such as stainless steels. In contrast, using diaphragms, the liquid acidic or alkaline electrolyte must be supplied in the anodic and cathodic compartment. In this case all cell components are exposed to the corrosive liquid electrolyte. Liquid acids for this configuration are usually avoided as only few and expensive materials such as the platinum metal group show acceptable corrosion resistance at low pH (Section 4.1). Compared to liquid acids, liquid alkaline electrolytes are less corrosive to cheap and abundant transition metals such as Ni, Fe and Co (Section 4.1), which thus can be used for cell and system components. Typically aqueous KOH solutions are used as liquid alkaline electrolytes, as these show the largest conductivities by hydroxide ions.

In cells with liquid electrolytes, the electrodes are typically directly connected or welded to the bipolar or end plates. In cells with SPE, current collectors are typically used to electrically contact the bipolar plates to the electrodes and to compensate their weak in-plane conductivity. The current collectors can be realized by porous and electron conducting materials such as carbon or metal foams, fleeces, or sintered bodies. The bipolar plates and the sides of the end plates that face the electrodes typically show textured structures. The supplied water (electrolyzer with SPE) or liquid electrolyte (electrolyzer with diaphragm) is typically purged in separated circulation loops along the electrodes through the textured structure of the bipolar plates. Accordingly, the gases produced in the cell are carried by convection of water/electrolyte to the gas outlets. Alternatively, the ascending bubbles by the gas evolution can drive the circulation without using a pump. In gas separators, the produced gases are separated from the supply water/electrolyte.

Water electrolysis with porous diaphragms is limited to balanced pressure operation (equal cathodic and anodic pressures), as differential pressures result in extensive cross-permeation of the electrolyte and dissolved gases [23]. In contrast, water electrolysis with gas-tight SPEs membranes can also be conducted at high differential pressures [24]. The alkaline SPEs thus far developed suffer from low durability, while acidic SPEs such as Nafion, a perfluorated sulfonic acid, are more durable and more conductive. Thus, state-of-the-art industrial alkaline water electrolysis is typically conducted with liquid lyes as the electrolyte.

In acidic electrolytes, protons permeate from the anode to the cathode during water electrolysis, while in alkaline electrolytes hydroxide ions permeate in the opposing direction. The ion conduction between the electrodes leads to convective water transport. Moreover, the amount of water that is consumed by the electrochemical water decomposition and water vapor in the product gases must be refilled into the system to avoid drying out. When level differences of water/electrolyte between the anodic and cathodic gas separators are balanced, the mixing of the anolyte and catholyte can display a source of gas crossover, which should ideally be avoided by degassing of the transferred water/electrolyte at atmospheric pressure [25,26].

3. ELECTROLYTES AND SEPARATORS

The electrolyte provides the ionic conductivity between the electrodes and within their porous structures. When a liquid electrolyte such as an aqueous solution of KOH is used, a porous separator (diaphragm) is typically employed in order to separate the oxygen and hydrogen evolved in the anodic and cathodic compartment. This porous separator is filled with the liquid electrolyte in order to enable the ionic conduction between the electrodes. When a SPE membrane is used between the electrodes, this membrane simultaneously provides the ionic conductivity and separates the gases.

3.1. Transport properties

Ohmic drop - Ion conduction in aqueous electrolytes is typically of ohmic character, which means that the ohmic voltage drop U_{Ω} in the electrolyte is proportional to the current. To describe the cell properties independent of the cell size, the current is typically normalized to the cell area leading

to the current density j . With a homogenous separator or SPE of thickness d between the electrodes, its Ohmic drop U_{sep} is related to its conductivity κ by:

$$U_{sep} = \frac{d j}{\kappa} \quad (8)$$

A detailed analysis of the ohmic drops during water electrolysis showed that the ohmic drop of the ion conduction through the separator dominates the overall cell resistance of state-of-the-art cells [27].

Gas diffusion - During water electrolysis, the separated evolved hydrogen and oxygen lead to concentration differences between the electrodes. Diffusion fluxes of both gases in the opposite direction of their concentration gradient result, respectively. Accordingly, hydrogen diffuses from the cathode to the anode while oxygen diffuses from the anode to the cathode. The mole flux density Φ_i^{Fick} (in units of $\text{mol s}^{-1} \text{cm}^{-2}$) of a gas i in an electrolyte that is caused by the diffusion can be derived on the basis of Fick's law to [28]

$$\Phi_i^{Fick} = -D_i \frac{\Delta c_i}{d}, \quad (9)$$

where D (in units of $\text{cm}^2 \text{s}^{-1}$) denotes the diffusion coefficient and Δc_i the concentration difference over the distance d . In the case of a water electrolyzer, the distance d refers to the distance between the electrodes [29] (typically to identify with the separator/membrane thickness). In equilibrium, Henry's law describes a linear relation of the concentration c_i of a dissolved gas in an electrolyte to its partial pressure p_i in the gaseous phase:

$$c_i = S_i p_i \quad (10)$$

The proportionality constant equals the solubility S_i (in units of $\text{mol cm}^{-3} \text{bar}^{-1}$). The latter equations can be combined to [29]

$$\Phi_{H_2}^{Fick} = -\frac{D_i S_i}{\varepsilon_i^{Fick}} \frac{\Delta p_i}{d}, \quad (11)$$

where Δp_i denotes the partial pressure difference and ε_i^{Fick} the diffusivity (or Fickian permeability). Analogously to the conductivity, the diffusivity, diffusion coefficient and solubility are material properties that are independent of the geometry of the considered medium. The diffusivity thus describes how permeable an electrolyte, separator or membrane is to gases.

Differential pressure electrolyte permeability - Besides diffusion, also differential pressures between the anodic and cathodic compartment can act as a driving force for the hydrogen and oxygen cross-permeation. Porous separators are typically permeable to gases and the liquid electrolytes at differential pressures [23], while with SPE membranes the influence of this mechanism on the overall gas crossover is negligible [30]. When the electrolyte is pushed through the porous structure of a separator during water electrolysis, it can carry dissolved gases [23]. In the case of a higher cathodic than anodic pressure, hydrogen is carried with the electrolyte from the cathode to the anode. In the case of higher anodic than cathodic pressures, oxygen is carried in the opposing direction (from the anode to the cathode).

3.2. Porous Separators

The porous structures of separators must be filled with aqueous electrolytes in order to provide ionic conductivity. In a water electrolyzer cell, this aqueous electrolyte can be provided in the anodic and cathodic compartment. Aqueous solutions of KOH are typically used for alkaline water electrolysis, as these are more conductive than other alkali metal bases (with respect to the same molarities). As discussed in Section 2, the corrosion of abundant metals for the cell and system components is an obstacle for the realization of water electrolysis with liquid acids. Accordingly, here we focus on diaphragms for usage in alkaline water electrolyzers.

Generally, following properties of porous separators are desirable, which will be discussed in Section 3.6 in more detail:

- Porosity and high wettability that allow the filling of the porous structure with the electrolyte [31].
- Small pore diameters to avoid the penetration of bubbles into the diaphragm and to reduce the differential pressure driven electrolyte permeability [23].
- High electrical resistance to avoid parasitic currents caused by electron conduction between the electrodes [32,33].
- Thin materials, in order to provide a small ohmic drop by the ion conduction [27].
- High volume fraction of pores to enable high ionic conductivity.
- High flexibility, so that the diaphragm does not break during operation or cell assembly [32].
- Mechanical form stability, so that the porosity is retained.
- Chemical durability for a long service life.

A variety of different materials are suitable for the usage as diaphragms in alkaline water electrolyzers. In the following, a selection of diaphragms reported for the usage in alkaline water electrolyzers is recapitulated, while more detailed reviews written in the 1980ies of the different types of diaphragms are provided in the literature [5,34]. (i) Asbestos: Asbestos is a silicate mineral in the form of fibrous crystals and was used over several decades as diaphragm in industrial water electrolyzers [32]. Its toxicity, thickness in the mm scale [5] and poor conductivities led to its replacement by other separator types. (ii) Porous ceramics: Ceramics show excellent wettability and excellent form retaining properties due to their stiffness. However, a lack of flexibility can be an issue with these types of materials. Divisek et al. [32] introduced diaphragms, where nickel oxide was deposited on nickel meshes. Using this configuration, mechanical flexibility was realized, however, these diaphragms were semi conducting and their lifetime was limited. In the last decade, procedures to produce flexible porous zirconia (ZrO_2) based porous thin foils were reported [35–38]. These materials may be promising for application. (iii) Polymers: Polymers typically show small contact angles in the order of 100° and consequently poor wettability of porous structures [39]. By surface functionalization with polar groups the poor wettability can be compensated, as studied for ultrafiltration polymer membranes in detail (see for example reference [40,41]). An advantage of porous polymers is their high flexibility and the ability to fabricate thin separators, while their thermomechanical floating at high temperatures and pressures displays an issue for the form stability. Polysulfone is a suitable polymer to realize diaphragms, as it is stiff, chemical resistant to hot alkaline

solutions and shows with 186°C [42,43] one of the highest glass transition temperatures among common commercially available polymers. (iv) Composites of polymers and ceramic filler: Porous composites of polymers and ceramic filler combine the mechanical flexibility of polymers with the wettability and the shape retaining stiffness of ceramics [4]. The most prominent material of this class is Zirfon [31], a composite material of Zirconia and polysulfone, that was introduced in 1995 [44]. A commercially available realization of this type of porous separator is nowadays produced by Agfa [45].

3.3. Polymer electrolyte membranes

In SPEs, ionizable functional groups are embedded in a polymer matrix. The polarities of these functional groups cause water uptake of SPEs when in contact with liquid water or water vapor [46–48]. The water uptake typically leads to an aqueous phase that is separated from the solid polymeric phase in the form of channels [49,50]. The functional groups provide either mobile protons or mobile hydroxide ions that can be dissolved in the aqueous phase. The charge of these mobile ions is balanced by opposing charged ions of the functional groups that are covalently bonded to the polymer matrix. Thus, in contrast to diaphragms, the ions responsible for the ionic conductivity are intrinsically provided. The water uptake and the concentration of the functional groups both display important parameters for the resulting conductivity and gas diffusivity of the SPE [46–48]. The most prominent representative of polymer electrolyte membranes displays the commercially available Nafion [51], a perfluorinated sulfonic acid. The structure and the phase morphologies of this material were rigorously examined over several decades using small-angle scattering techniques [50,52]. Allen et al [53] recently used 3-D electron tomography to resolve the phase separation between the aqueous and solid phase and showed that the water channels have a diameter of approximately 2.5 nm.

In acidic SPEs, the functional groups are typically realized by sulfonic acid groups ($-\text{SO}_3\text{H}$) [48,54,55]. These materials are typically stable in aqueous solutions. However, hydrogen and oxygen cross-permeation lead to hydrogen peroxide or radical (H^\bullet , OH^\bullet and OOH^\bullet) production at the catalysts in electrolyzers [56,57]. The effect of chemical degradation of acidic SPEs was examined in more detail for polymer electrolyte fuel cells [58–61], in which the membranes are exposed to a similar chemical environment in comparison to water electrolyzers. Perfluorinated sulfonic acids are most commonly used in fuel cells and water electrolyzers, as these materials show the best chemical resistance to the harmful radicals [54]. Moreover, these materials provide high proton conductivity. Alkaline SPEs with a variety of functional groups and polymeric backbone structures were developed as discussed in several reviews [62–64]. However, all these functional groups are attacked by the alkaline environment that is provided by the mobile hydroxide ions they provide. This intrinsic instability of alkaline SPEs displays a challenge to be solved when aiming at industrial applications. For this reason, alkaline SPE membranes will not be considered in detail in this review. Via ion exchange, the mobile ions in SPEs can be replaced by other ions which have the same sign of charge [65–67]. Accordingly, SPEs with mobile cations are commonly referred to as cation exchange membranes, while those with mobile anions are commonly referred to as anion exchange membranes.

Polymer electrolyte membranes are typically manufacturable in different thicknesses. Generally, following properties of polymer electrolyte membranes are desirable [27]:

- High conductivity.
- Low gas permeability.
- High chemical stability.
- High thermomechanical resistance to avoid creep under elevated temperature and pressure.

Alkaline water electrolysis with a liquid electrolyte can also be realized by replacing the porous separator with a SPE membrane. In the case of hydroxide conducting SPEs, the intrinsic conductivity of the SPE can be enhanced when lyes penetrate into the water channels of the SPE [68]. Moreover, cation exchange membranes can be used as the separator in the alkaline water electrolyzers, where the protons of the functional group are replaced by the alkali metal ions from the liquid lye [69]. In this case, the hydroxide ions from the liquid electrolyte supply ionic conductivity. However, this configuration leads to a poor conductivity that is in the range of 100 times smaller than that of the pure hydroxide solutions [69]. This poor conductivity may result from a reduced electrolyte uptake and the interaction of the ions in the aqueous phase.

3.4. Physical properties of electrolytes

The aqueous phase in both, diaphragms and SPEs is responsible for the ion conduction. In comparison to pure aqueous solutions with the same composition as the aqueous phase in the water channels of SPEs, the morphology of the water channels in the form of reduced volume fraction and tortuosity reduce the overall conductivity [70]. In the following, the mechanisms of the ion conduction and gas permeation in aqueous electrolytes are discussed. In Section 3.6, these properties are used to compare the properties and of liquid electrolytes and SPEs. Alkaline SPEs are due to their lack of stability not considered.

Viscosity - The diffusion coefficient of a molecule, ion or particle i in a liquid solution is directly correlated to the viscosity of the medium. In the physical picture, the viscosity influences the friction of the Brownian motion. Thus, (with respect to the same amount of charge carriers) the ionic conductivity and gas diffusivity both typically decrease towards higher viscosities. The viscosity of aqueous solutions typically decreases towards higher temperatures. Figure 2 graphs the viscosity of water, KCl, KOH and HCl as a function of concentration and temperature. In these solutions, potassium cations and chloride anions influence the viscosity in a similar manner, respectively, as these ions are of approximately equal weight and absolute value of charge. Accordingly, the higher viscosity of KOH solutions than HCl solutions can be mainly attributed to different influences of hydroxide and protons on the water bond network.

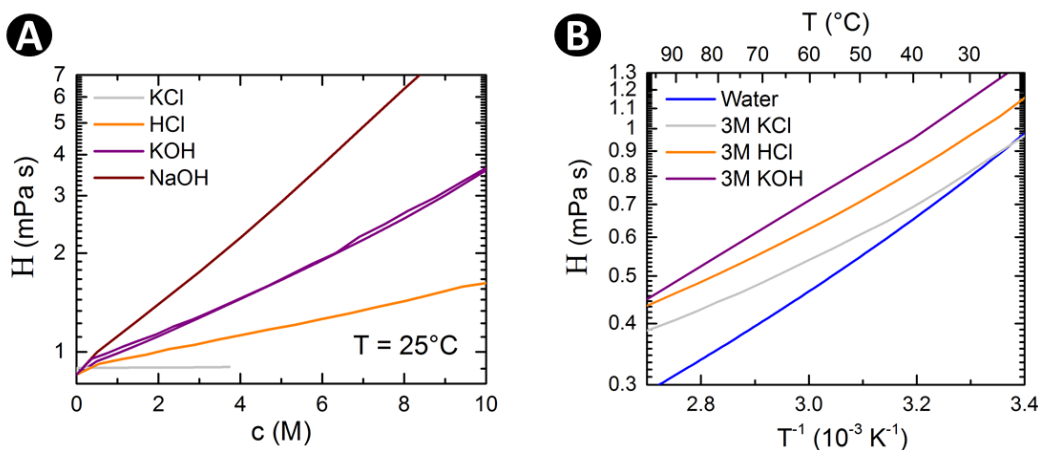


Figure 2. (A): Viscosity H of aqueous solutions of NaOH (Data from reference [71]), KOH (data from reference [72] and [71]) and KCL (data from reference [72]) as function of the concentration at 25°C . (B): Viscosity H of water (data from reference [73]) and aqueous solutions of 3M KCl, KOH, HCl (data from reference [72]) in a modified Arrhenius-plot, where a logarithmic scale of H is used instead of $\ln(H)$.

Proton and hydroxide conduction - Proton and hydroxide conduction in aqueous solutions takes place by two mechanisms: (i) The vehicle mechanism, where protons or hydroxide ions permeate as solvated ions through the aqueous solution [74]. (ii) The Grothuss mechanism [74–76], where protons are exchanged along the hydrogen bond network of water molecules.

Higher temperatures enable a more frequent thermally activated proton exchange and reduce the viscosity of the electrolyte, increasing the ion mobility and thereby the conductivity. Empirically, it is a well established fact that the mobility of protons in aqueous solutions is higher than that of hydroxide ions, which means that with respect to the same concentrations acids are typically more conductive than bases. At 25°C , the mobility of protons is reported to be 1.77 higher than that of hydroxide [77]. On a microscopic level, Uddin et al. [74] described these differences between the mobilities using molecular dynamic studies.

The ion motion by the Vehicle mechanism leads to the convection of water molecules, commonly referred to as electro-osmotic water drag [78]. In the case of Nafion membranes immersed in water, 3 to 5 water molecules were reported to be carried along with each proton that passes through the membrane [28,78,79]. In liquid solutions, the convective water transport results in height differences of the electrolyte that are typically instantaneously compensated by the gravimetric force.

The ionic conductivity of aqueous electrolytes increases with concentration until interactions by Coulombic force between the ions in the electrolyte reduce the conductivity [19]. Figure 3 shows the conductivity of hydrochloric acid (HCl) and potassium hydroxide (KOH) as a function of the molarity for different temperatures. Among all aqueous solutions of alkali metal hydroxides, potassium hydroxide shows the largest conductivity and thus displays the preferred electrolyte for alkaline water electrolysis. In hydrochloric acid and potassium hydroxide, the counter ions (chloride and hydroxide) are of approximately equal weight and equal absolute value of charge. Thus, both ion species show approximately equal mobility [19]. Hydrochloric acid is here graphed as a representative for acids

(despite its use as electrolyte for water electrolysis is not suitable as chloride ions are oxidized to chlorine at the anodic potentials during water electrolysis). Alkaline electrolysis is typically conducted with 5 to 7 molar (25-30wt%) KOH solutions, as these show the largest conductivities.

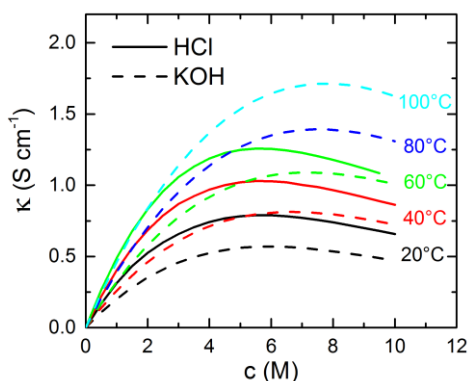


Figure 3. Conductivity of KOH (dashed lines, extracted from reference [80]) and HCl (solid lines, extracted from reference [81]) as a function of the concentration for different temperatures.

The ionic conductivity of aqueous solutions is typically measured using impedance spectroscopy or the current interrupt technique. Using these techniques, all mobile ions in the electrolyte move in the applied alternating electric field [70]. However, during water electrolysis at direct currents only protons or hydroxide ions are exchanged between the electrodes [27]. The counter ions in the electrolyte are not involved in the reaction and thus do not contribute to the current at stationary conditions, while they contribute to the alternating currents. Thus, using the measurement techniques discussed above the alternating current (AC) conductivity is measured, while the direct current (DC) conductivity is decisive for the Ohmic drop during water electrolysis [27]. In the case of cation exchange SPEs, the cations are mobile, while the anions are covalently bonded to the polymer matrix and thus not moveable [70]. Accordingly, in polymer electrolytes the AC conductivity equals the DC conductivity during water electrolysis (if all cations are protons [70]). In contrast, with aqueous electrolytes, all ions contribute to the AC conductivity while only the protons or hydroxide ions contribute to the DC conductivity during water electrolysis [27].

In the case of Nafion in contact with liquid pure water (defined as the fully hydrated state), water uptakes in the range from 20 to 26 water molecules per sulfonic acid group were reported [82–85]. These water uptakes can be calculated to lead to a proton concentration in aqueous phase in the range from 2.1 to 2.8 mol/l [70]. The proton conductivity of Nafion was measured to approximately 0.16 times that of liquid acidic aqueous solutions with 2.8 mol/l [70]. This difference was attributed to the influence of the microscopic morphology on the overall conductivity, while the proton mobility in the aqueous phase of Nafion immersed in water and that in aqueous solutions were estimated to be similar [70].

The conductivity of KOH inside the channels of porous separators is typically equal to that of bulk KOH [27]. As discussed above, the hydroxide mobility is decisive for the Ohmic resistance during alkaline water electrolysis, while the cation mobility is not expected to contribute to the DC

conductivity. *Figure 4* shows the ionic conductivities of Nafion, HCl, and KOH. Moreover, in this figure the proton and hydroxide ion conductivities of these solutions (by subtracting the contributions of the counter ions to the conductivity by the procedure described in reference [27,70]) were graphed. At 80°C, approximately equal conductivities of protons in the aqueous phase of Nafion and hydroxide ions in a 7 M solution of KOH. Moreover, in Nafion and Zirfon the geometric impact of the morphology of the aqueous phase on the overall conductivity was estimated to approximately the same extent [23,70]. Thus, Zirfon with 7M KOH filling and Nafion show approximately equal conductivities [27].

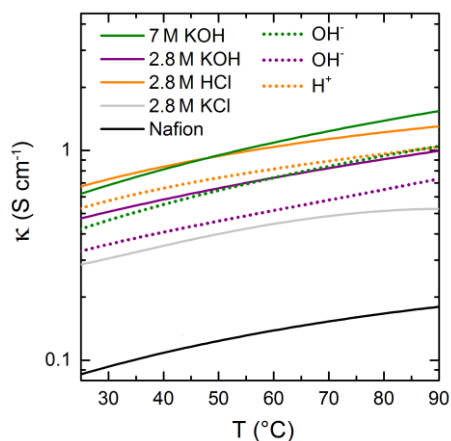


Figure 4. Conductivities of different electrolytes. Data for Nafion and 2.8 M KCl and HCl from reference [70]. Data for the KOH solutions from reference [80]. The concentrations of 2.8 M refer to that of the protons in the aqueous phase of Nafion [70]. Solid lines: Based on measurements (data from reference [70,80]). Dotted lines: Proton or hydroxide conductivity for the respective concentrations as estimated by multiplying with the transfer number [27,70].

Gas diffusivity - With reference to equation (11), the gas diffusivity is the product of the diffusion coefficient and solubility. Hydrogen and oxygen are both non-polar diatomic gases, and accordingly, the mechanisms of their diffusion and solution in aqueous solutions are similar. The temperature dependencies of their diffusion coefficient, solubility and diffusivity in aqueous solutions can be approximated by the Boltzmann distribution (equation (6)).

Figure 5 shows the solubility of oxygen in sulfuric acid, phosphoric acid, and potassium hydroxide. Higher electrolyte concentrations decrease the oxygen solubility. The decrease of the oxygen solubility towards higher electrolyte concentrations is in the case of potassium hydroxide solutions stronger than in the case of the acidic solution. Approaches to describe the influence of the concentration on the solubility were derived on the basis of electrostatic calculations. Ruetschi et al. [89] reported that the influence of the proton concentration on the gas solubility is negligible, while hydroxide ions dramatically reduce the gas solubility.

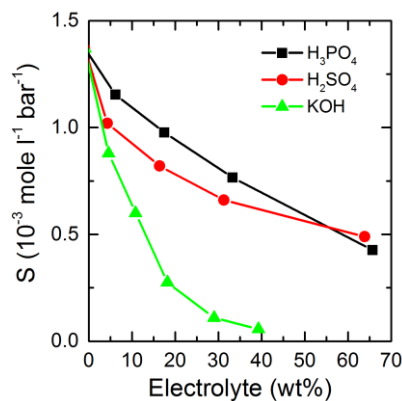


Figure 5. Oxygen solubility in alkaline and acidic electrolytes as a function of the weight composition of the electrolyte. The data in this graph is replotted from reference [87].

In the case of KOH, the effect of temperature and molarity on the hydrogen and oxygen diffusion coefficient was measured in detail by Tham et al. [88]. This study showed that the diffusion coefficient increases towards higher temperatures, while it decreases toward higher concentrations. This behavior can be directly correlated to the inverse of the viscosity [23]. The hydrogen and oxygen diffusion coefficients and solubilities decrease toward higher concentrations of the electrolytic solutions. As a result, the gas diffusivity also decreases toward higher electrolyte concentrations.

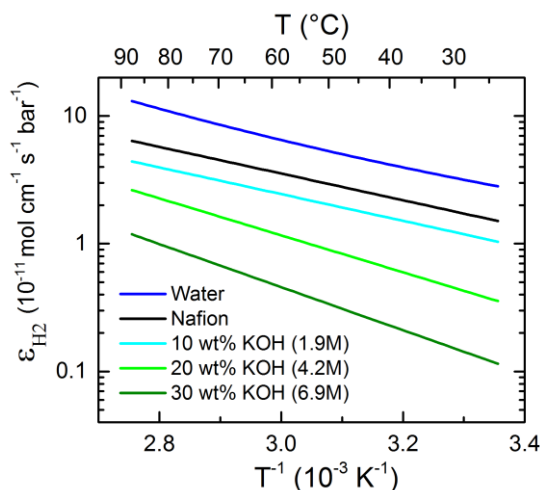


Figure 6. Hydrogen diffusivities in different electrolytes. Based on the data reported in [23,70].

Acids show typically higher gas diffusivities than bases with respect to equal molarities. This difference is ascribable to higher diffusion coefficients (related to lower viscosities) of the gases in acids than that in comparison to bases. However, more importantly, the hydrogen and oxygen solubility in alkaline solutions is drastically lower than in acidic solutions. Figure 6 shows the hydrogen diffusivity in Nafion, water and KOH solution with various molarities. The hydrogen diffusivity in Nafion is approximately 50% of that of water, while conductivity was above discussed to 16% of that of an aqueous solution with similar proton concentration. This extra diffusivity was

ascribed to the high hydrogen and oxygen diffusivity in the solid phase [89]. Water penetrating into the polymer matrix of Nafion acts as a plasticizer that increases the permeability of the solid phase [89]. In the case of Zirfon, the hydrogen diffusivity in the solid phase was estimated to be negligible [23]. The combination of high diffusivities of the solid and aqueous phase in Nafion results in an approximately 38-times larger hydrogen diffusivity of Nafion than of Zirfon filled with 30wt% KOH at a temperature of 80°C [27], while both materials show almost equal conductivities [27].

3.5. Gas evolution and bubble formation

Electrochemical water splitting leads to the phase transition of liquid water to the gaseous products in the form of hydrogen and oxygen. Figure 7 shows that the concentration of gases in the gaseous phase (approximated by the ideal gas law) is at least 60 times higher than that of dissolved gases in water (approximated by Henry's law) with respect to the same partial pressures in the gaseous phase. The pressure inside a bubble increases inversely proportionally to the bubble diameter. When the concentrations of gases exceed their saturation solubilities, dissolved gases can form bubbles. However, at the non-equilibrium situation of electrolytic gas evolution, the concentration of evolved gas in the dissolved state can be higher than under equilibrium conditions. This effect is commonly referred to as supersaturation [90–94]. The complex physics of the non-equilibrium process of the bubble formation are difficult to describe by macroscopic models and exceed the scope of this review.

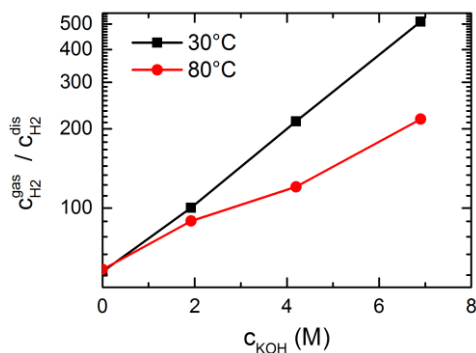


Figure 7. Relation of the hydrogen concentration in the gaseous phase to that dissolved in aqueous KOH solutions as a function of KOH molarity. Concentrations of the gaseous phase are calculated based on the ideal gas law. The concentrations of dissolved hydrogen are calculated by Henry's law and the hydrogen solubility in KOH reported in [86].

3.6. Comparison of porous separators and SPEs

The ion conduction and gas diffusion through porous separators and membranes depend on the morphology of the aqueous phase and its composition. Whereas the ion conduction through the solid phase is negligible, its gas diffusivity significantly influences the overall gas cross-permeation [23,89]. The following comparison is focused on aqueous KOH solutions in combination with porous separators and acidic SPEs. Quantitative values for the physical properties of both types are discussed

for Zirfon (Agfa) as a porous separator and Nafion (DuPont) as an acidic SPE, representing the state-of-the-art materials.

Structure - In a SPE membrane, the ionic charge carriers are intrinsically provided, while water must be taken up by the membrane in order to dissolve these ions in an aqueous phase. A porous separator has to be filled with a liquid electrolyte in order to provide ionic conductivity. In both, SPE membranes and diaphragms, the aqueous phase for the ion conduction is embedded in a porous framework. The pores of the Zirfon separator are with circa 150 ± 50 nm [45] almost two orders of magnitude larger as those of the Nafion membrane with 2.5 ± 0.5 nm [53]. Volume fraction of the hydrophilic phase was reported to 55% of Zirfon [45] and 56% for Nafion [53].

Mechanical properties - The mechanical stability of polymers represents a major factor that limits the temperature range of electrolyzers with polymer based materials. The glass transition temperature of Nafion is in the order of 100°C [95]. Below this temperature, the polymer can slowly float under pressure, which leads to an irreversible plastic deformation [96–99]. Additionally, during operation, the water uptake of Nafion membranes decreases their mechanical strength [83] as water acts as a plasticizer. Accordingly, the mechanical properties of SPEs are expected to display an issue for the durability. In the case of the Zirfon separator, the polysulfone matrix has a glass transition temperature of 186°C [42,43]. With respect to this high glass transition temperature and the formstable Zirconia filler, mechanical issues and plastic deformation of the separator are expected to be a minor issue for operation temperatures below 100°C .

Permeability to differential pressures - The differential pressure permeability of the separator/membrane to gases and water mainly depends on the friction at the electrolyte-polymer interface. Smaller pores increase the friction of the permeation and thus decrease the permeability [23]. Besides the pore diameter, also the intermolecular forces between the solid and aqueous phase (as described by the contact angle) display an important parameter for the friction. Differential pressure was measured to negligibly influence the gas crossover through Nafion membranes [30]. In contrast, the gas crossover with Zirfon separators was shown to be dominated by the differential pressure forced permeation [23]. These differences originate from the approximately two orders of magnitude larger pore diameters of Zirfon separators than those of Nafion membranes.

The pore diameter also displays important parameter for the bubble repulsion of the separator/membrane. At the interface of the gaseous phase (in the form of bubbles) to the wetted solid phase of the separator/membrane, the capillary pressure of the electrolyte in the pores of the separator represents a repulsive force that avoids the penetration of the gaseous phase into the pores [23]. The capillary pressure of the aqueous phase in a pore is approximately reciprocally proportional to its radius. When the pores are smaller than the diameter of a evolved bubbles at the electrodes, the bubbles cannot penetrate into the pores of the separator/membrane [23]. As discussed in Section 3.5, the concentration of hydrogen or oxygen in the gaseous phase is at least 60 times larger than that as dissolved molecules in aqueous solutions. Accordingly, bubbles that are carried by differential

pressure forced electrolyte cross-permeation through the pores drastically increase the gas crossover [23].

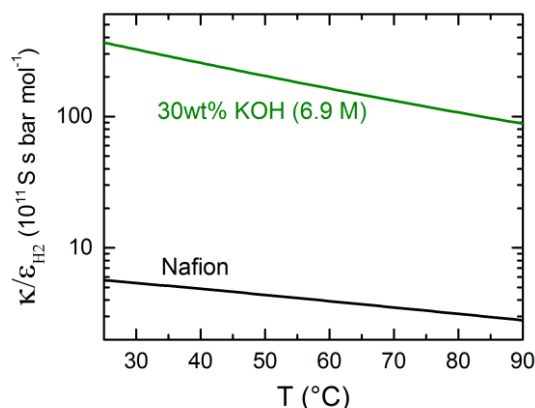


Figure 8. Ratio of DC-conductivity to hydrogen diffusivity of a 6.9M KOH solution (30 wt%) and Nafion extracted from the data graphed in Figure 4 and Figure 6.

Ratio of conductivity to diffusivity - As later discussed in Section 6, the thickness of the separator/membrane relates Ohmic losses to the losses caused by the gas crossover. A higher ratio of conductivity to gas diffusivity means that smaller Ohmic drops and higher gas purities can be achieved in the cell. Figure 8 shows this ratio for Nafion and 7M KOH. At 80°C, the ratio of conductivity to diffusivity is approximately 38 higher for the 30wt% KOH solution than that of the Nafion membrane. The ratio decreases towards higher temperatures as the diffusivity increases faster than the conductivity. In the case of porous separators with impermeable solid phases, the ratio of the conductivity to the diffusivity is independent of the microscopic structure, as the aqueous phase is responsible for both properties.

3.7. Section summary

In the case of a porous separator, an electrolytic solution must penetrate into its pores to provide ionic conductivity. In the case of SPEs, the charge carriers are intrinsically provided by functional groups. By water uptake of SPEs an aqueous phase is formed, in which the charge carrier ions (either protons or hydroxide ions) are dissociated. In both, porous separators and SPE membranes, the ion conduction takes place in aqueous phases. The highest conductivities of acidic and alkaline aqueous electrolytes are typically between 4 to 8 molar solutions and thus should be aimed for the aqueous phase in water electrolyzers. Alkaline solutions typically show smaller gas diffusivities than acidic solution, which means that potentially higher gas purities can be achieved with alkaline than with acidic electrolytes. However, the main disadvantage of porous separators filled with liquid electrolytes can be attributed to the differential pressure driven gas and electrolyte permeation, which is negligible for SPE membranes such as Nafion.

4. ELECTROCATALYSTS

Aqueous solutions with proton or hydroxide concentrations in between 4 and 8 mol display the highest conductivities and are thus typically used in water electrolyzers. These concentrations correspond to pHs of below -0.5 or above 14.5, respectively. The electrocatalysts in water electrolyzers are typically directly exposed to such harsh electrolytes.

4.1. Stability

Stability of electrocatalysts in water electrolyzers is important to achieve long operating life. Electrochemical corrosion at the interface of a metal to an electrolyte displays the main stability issue of electrocatalysts, while also structural transformations of electrocatalysts can lead to severe degradation.

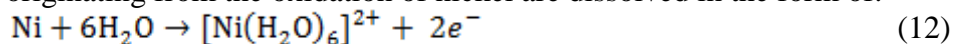
Metal surfaces in contact with aqueous solutions - When metals are exposed to a medium, the unpaired electrons of the atoms at the metal surface interact with this medium. In the case of an aqueous solution that is in contact with a metal, the surface metal ions can (i) adsorb atoms, ions or molecules that occur inside the electrolyte, (ii) can form a passivation layer or (iii) can be dissolved into the electrolyte. The adsorption of species from the electrolyte is the first step of a catalytic reaction. In case (ii) and (iii) the ions of the metal are oxidized.

Passivation layers - In passivation layers, the surface atoms of the metal are oxidized forming stable covalent or ionic bonds with oxygen [100]. Moreover, mainly in alkaline electrolytes, hydroxides (OH) or oxy hydroxides (OOH) can be incorporated into passivation layers [101–103]. The chemical composition and oxide structure of the passivation layer of a metal depend on pH [104], the potential difference between the metal and the electrolyte [101,105,106], temperature [105,106], and dissolved species in the electrolyte, such as gases or ions etc. For instance, traces of chloride in the electrolyte can lead to the dissolution of oxide layers that are stable in chloride-free electrolytes [107,108]. The thickness of the passivation layer depends on the stability of the formed oxide as well as its porosity. For instance, in the case of iron, the porous iron oxide passivation layer is steadily growing at near neutral pHs [109]. In contrast, in the case of nickel, the passivation layer is more dense and was reported to the order of 10 nm [110–112].

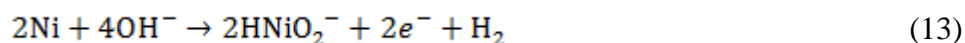
Dissolution - During electrochemical dissolution, metal atoms **M** are removed from a metal surface or passivation layer and dissolved as ions. In the solution, these ions are solvated (surrounded by the molecules of the solvent that are attracted by the electrostatic force). Depending on the electronic structures of the metal ions and the solvent, the metal ions can interact with solvent molecules in three different kind of electronic interactions: (i) Without formation of covalent bonds the metal ions can be dissolved as solvated cations in the form M^{x+} . For example, alkali metal or alkali earth metals are typically dissolved in this way. (ii) The metal atoms or ions form coordination complexes, where ligands are coordinated to them. The ligands can be ions or molecules (e.g.

molecules of the solvent). In contrast to the electrostatic forces between solvated ions and the solvent, in coordination complexes the metal ions and ligands form strong chemical bonds. The ligand field theory is typically used to describe the orbital interaction of the metal ion and the ligands. In the acidic regime, most transition metals are dissolved as coordination complexes, as for example iron or nickel in the form $[M(H_2O)_6]^{2+}$. The detailed chemistry of coordination complexes with its various different structures exceeds the scope of this review and will not be considered in more detail, for what reason we refer to textbooks that treat this topic in detail [113]. (iii) The dissolved metal atoms can react with electrolyte molecules forming covalent or ionic bonds. For instance, the dissolution of iron or nickel in the alkaline regime were reported to lead to ions in the form of HMO_2^- [114].

The reactions of the dissolution are in the following exemplified for non-passivated nickel. In acidic media, nickel cations originating from the oxidation of nickel are dissolved in the form of:



In the alkaline regime, the dissolved nickel forms anions, in which the nickel cations itself show the oxidation state +II:



In the case of passivated nickel, which can arise in stoichiometric composition such as NiO, Ni(OH)₂, Ni₂O₃, NiOOH, Ni₃O₄, the reactions are different, as described by Pourbaix [114] in detail.

The metals across the periodic table form different complexes in alkaline and acidic solutions, which show different saturation solubilities. Moreover, the solubility of metals and metal oxides depends on the composition of the solid phase. For example, as illustrated in Figure 9, the solubility of iron hydroxide Fe(OH)₂ is far higher than that of iron oxide Fe₂O₃ or iron oxy hydroxide FeOOH.

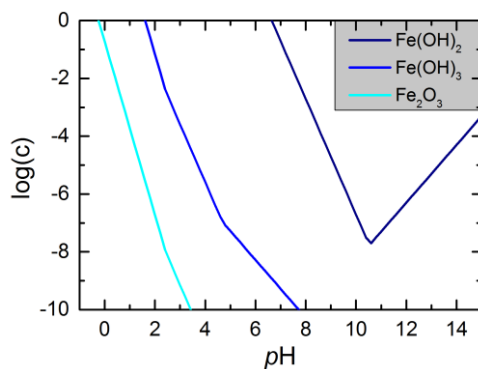


Figure 9. Logarithm of the saturation concentration of dissolved iron ions from different iron oxides/hydroxides as a function of pH. Reprinted based on the data published by Pourbaix et al. [114].

Electronic structure - Different corrosion behavior of metals is attributable to their different electronic structures and those of their oxides. Moreover, the morphology and crystallographic structure of the oxides is decisive for the passivation and corrosion. In vacuum, the work function characterizes the energy required to extract an electron from the surface of a metal [115,116]. When the metal is in contact with an electrolyte, the lowest potential at which the ions at the metal can be oxidized is characterized by the nobleness, which is tabulated in the electrochemical series with

reference to acidic solutions (without complexing agents) for a pH of 0 [117]. Comparing both cases, the contact of the metal surface with vacuum or an aqueous solution, the electronic interaction with water molecules and dissolved species such as ions and gases displays the main difference. Accordingly, despite the work function and nobleness roughly correlate, the electronic interactions between the metal surface and the electrolyte yield differences for the trends of work function and nobleness [118]. For example, the highest work function of all pure metals shows platinum [116], while gold is the noblest of all metals [117]. Another important property to characterize a metal in an aqueous solution is the potential of zero charge [119]. The potential of zero charge can be related to the energy necessary to extract electrons from the Fermi level of the metal covered with a water layer.

The bulk electronic structure of metals with an ordered lattice (continuous boundary conditions) can be analytically calculated by the band theory (a standard method in solid state physics). However, at the surface of the metals, the continuous boundary conditions and thus the symmetry required for the analytical band theory calculations are broken. Accordingly, numerical quantum mechanical calculations are typically used to describe the surface of metals. When atoms or molecules are bonded onto the surface, these adsorbed species influence the electronic structure at the surface.

Hammer and Norskov modeled the electronic interaction of metal surfaces with adsorbed hydrogen using a computational density functional theory (DFT) model [118]. Figure 10 illustrates the modeled density of states (energy distribution of electrons) of this work at the (111) surfaces of Ni, Cu, Pt, and Au with and without hydrogen adsorption. On the basis of this simulation, the authors attributed the higher nobleness of gold in comparison to platinum (despite the larger experimental value of the work function of platinum) to the higher degree of filling of the antibonding orbitals and to minor overlap of valence orbitals between metal and adsorbed hydrogen. A similar relation results if one compares Ni with Cu, where Ni exhibits higher work function, although its oxidation potential is lower in comparison to Cu. In fact the degree of filling of antibonding orbitals determines bond strength of adsorbate at the metal surface (the higher is the filling the weaker bond becomes) while the degree of valence orbital overlap influences activation barrier (the smaller is the overlap the larger is the activation energy for the adsorption process).

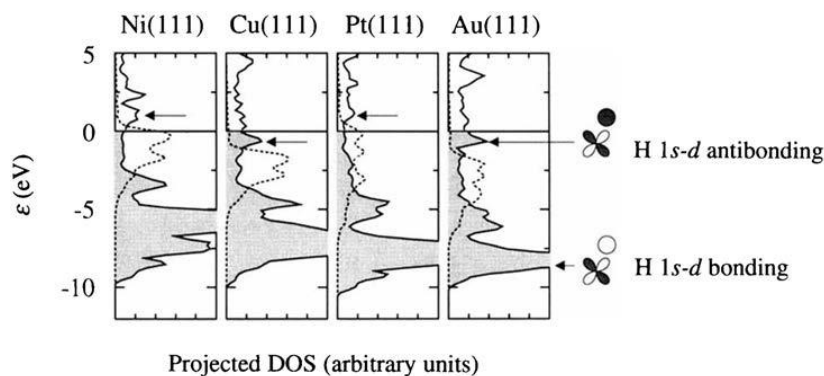


Figure 10. Projected density of states for four different metals with the (111) surface reported by Hammer and Norskov [118]. Dotted line: Pure metal. Solid lines: Interaction with a hydrogen atom. The arrow indicates the antibonding surface states. Reprinted with the permission of the Nature Publishing group.

Pourbaix diagrams - The process of corrosion is accompanied by a phase transition and thus a change in Gibb's free energy. In the case of an electrochemical reaction, Gibb's free energy of the reaction can be divided by the Faraday constant times the number of electrons involved in the electrochemical reaction in order to calculate the equilibrium potential of the phase transition (commonly referred to as Nernst equation). Marcel Pourbaix established diagrams based on calorimetric and electrochemical data, where equilibrium potentials for the thermodynamically stable phases of a metal, its oxides and its dissolved ions are plotted against the solution pH [114]. Typically, the potentials in these diagrams are graphed relatively to that of hydrogen at standard conditions (defined as pH=0 and 25°C), commonly referred to as normal hydrogen electrode (NHE) or standard hydrogen electrode (SHE). In a monumental work, Pourbaix and co-workers derived these diagrams (which were later named after his inventor) for the metals across the periodic table [114]. In the case of pH dependent reaction, the reversible hydrogen electrode (RHE) is typically used as reference voltage, which refers to the equilibrium potential of hydrogen at the considered pH. The difference between the potentials as a function of pH can be calculated by:

$$E_0(\text{RHE}) = E_0(\text{NHE}) - \text{pH} * 0.059 \text{ V} \quad (14)$$

Most equilibrium potentials of reactions involving protons or hydroxide ions (such as the formation of an oxide) obey the same pH-dependence as that of the RHE. When protons or hydroxide ions are not consumed or produced in a reaction (as for example by the acidic dissolution of non-passivated nickel described by equation (12)), the potential vs NHE is typically pH independent (resulting in a horizontal line in the Pourbaix diagram).

Figure 10 shows the Pourbaix diagram of nickel. In the acidic regime, nickel dissolves to Ni^{2+} ions over a broad potential window. In alkaline electrolytes, nickel or its oxides/hydroxides are (above concentrations of 10^{-6} M nickel ions in the electrolyte) thermodynamically stable at the anodic and cathodic potentials during water electrolysis.

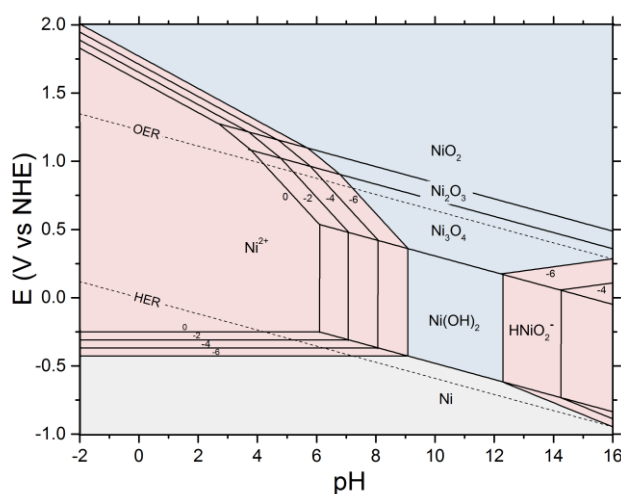


Figure 11. Pourbaix diagram of nickel, replotted using the equations reported in reference [114]. With reference to a concentration of dissolved Ni ions of 1 μM , the grayish area represents immunity against corrosion, the blueish area passivation and the reddish area dissolution.

Corrosion of metals across the periodic table - Figure 12 graphs thermodynamically stable phases of metals across the periodic table in the potential ranges of the water electrolysis reactions at pH = -0.5 and pH = 14.5, 25 °C and concentrations of dissolved metal ions of 1 μM, respectively. In this figure all potentials refer to the RHE. Above 1.23 V vs RHE (the equilibrium potential of the oxygen evolution reaction), except gold all metals are oxidized and thus must be protected by passivation layers in order to avoid their dissolution.

More metals are thermodynamically stable for the potentials below the HER and above OER in the alkaline regime in comparison to the acidic regime. In the case of acidic media, the oxides of the rare and costly Ir, Pt, and Rh are thermodynamically stable in the potential window between 1.23 and 1.6 V that typically occurs at the anode during water electrolysis. Moreover, some oxides of the left-side transition metals in the periodic table (Ti, Nb, Ta, and W) are thermodynamically stable in this potential range, which however show poor activity for the oxygen evolution reaction. Moreover, these metal oxides are typically insulators or bad conducting semi-conductors. The great advantage of alkaline regime is that the cheap and abundant Ni and Co are thermodynamically stable in the potential regions where the cathode operates during water electrolysis, while their oxides are thermodynamically stable for potentials applied at the anode. As discussed later, these metals show catalytic activity for both, the hydrogen and oxygen evolution reactions. To conclude, a variety of metals can be used as electrocatalysts, cell and system components for alkaline water electrolyzers, while in the case of acidic water electrolyzers, only few and costly materials are stable in the required potential range.

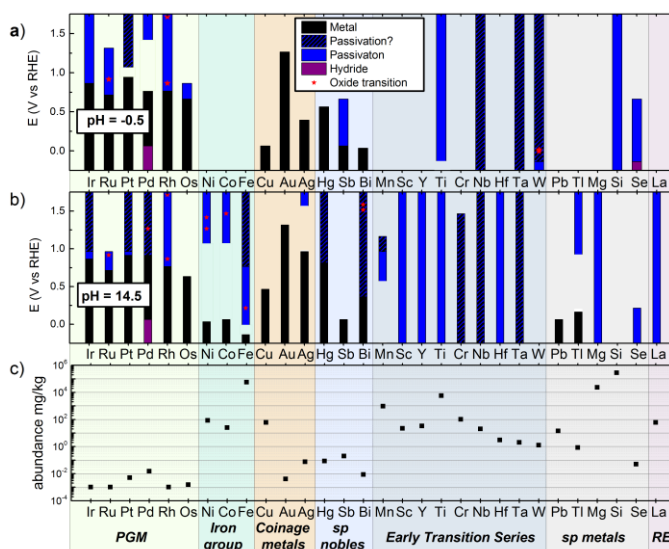


Figure 12. Chart for metals that show thermodynamically stable solid phases at pH -0,5 (a) or pH 14.5 (b), with reference to a temperature of 25°C and a dissolved metal ion concentration of 10⁻⁶ M or lower (based on the data reported by Pourbaix et al. [114]). The graphed potential refers to that of the reversible hydrogen electrode (RHE). Black area: Metallic phase stable. Blue area: Stable oxide. Shaded blue area: Not clarified if the oxide is stable. Purple: Stable hydride. (c) Mean abundance of the metals in the earth crust (in mg of metal per kg of earth’s crust). Data extracted from [120].

Kinetics of the dissolution - In the potential range that the thermodynamic data of Pourbaix predicts immunity, negligible dissolution rates of noble metals were measured [121,122]. If neither a metal nor its oxide is thermodynamically stable at a certain potential, the dissolution process is a question of the kinetics. For example, in the case of carbon, which is used in fuel cell as the catalyst support, the dissolution rate is below potentials of 0.5V negligible [123], although carbon is not thermodynamically stable above 0.2V vs RHE [114]. In contrast, copper rapidly dissolves in acidic solutions above its oxidation potentials (as utilized in industrial electrorefinery processes). At oxide transitions of metals high dissolution rates were reported and attributed to intermediate oxides during the formation and morphology changes of the surface [121,122,124].

During the oxygen evolution at a metal or metal oxide surface, the reaction involves changes of the oxidation states of the metal ions at the surface [102,126–131]. Accordingly, although various metal oxides with a defined composition such as IrO_2 are thermodynamically stable in the regime where the OER takes place, oxides with different stoichiometric composition occur during the OER [125]. It is questionable whether these oxides are stable. Binninger et al [132] concluded that metals oxides cannot be stable during the OER and that thus dissolution of metal catalysts for the oxygen evolution is inevitable giving pure thermodynamic reasons. Metal or metal oxide surfaces at which the OER takes place are considered to consist of amorphous structures in the form of hydrous oxides [130,131,133]. When a metal does not show an oxide that is thermodynamically stable in the potential range where the OER takes place, this metal can be expected to dissolve faster than other metals which have at least one stable oxide. Figure 13 shows the dissolution rate of Ir and Ru in perchloric acid as a function of potential and current density. The dissolution rates of both metals scale approximately exponentially with the potential. At a current density of 10 mA/cm², the dissolution rate of Ru is more than one order of magnitude higher than that of Ir.

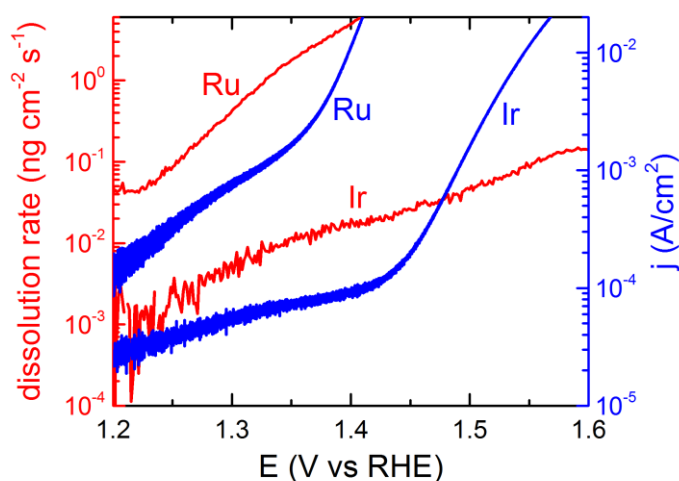


Figure 13. Dissolution rate (left scale) and current density (right scale) of plane and polycrystalline Ir and Ru samples during a forward scan of the potential with 2 mV/s in the potential region of the OER. Data extracted from [125].

Multielement electrochemical corrosion - In the case of alloys, the corrosion properties depend on the electrochemical properties of the pure alloy components, their spatial arrangement and

their electronic interaction [134]. A non-stable component can for example be leached out and then be passivated by a stable component [135]. Accordingly, when some species dissolved faster than others the elemental composition of an alloy changes over time. For example, in stainless steels iron is initially leached out of the surface layer while the Cr content on the surface increases and then finally passivates the alloy [136,137]. Moreover, alloying can result in changes of the binding energies of the atoms and the structure of the passivation layers [138,139]. These changes of the electronic structure can influence the oxidation potential and dissolution kinetics.

Structural transformation - Besides the electrochemical corrosion, structural transformations of electrocatalysts can occur during water electrolysis. Especially at the anode during the oxygen evolution, where the atoms on the surface permanently undergo changes of their oxidation states, changes of the crystal structure can introduce defects and mechanical stress. Surface segregation can lead to a low degree of surface homogeneity [140]. At the cathode, the formation of hydrides (which is especially relevant for nickel catalysts [141,142]), can also lead to mechanical stress and deformation. In addition, hydrogen embrittlement can lead to mechanical stress of the employed metals at the cathode [143–146]. Ostwald ripening [147,148] of high surface area electrocatalysts can occur, where small particles are dissolved and re-deposition on larger particles. The resulting agglomeration of the electrocatalyst leads to a loss of the electrochemically active surface area of the electrocatalyst. When the catalyst is attached to a support, changes of the passivation layer of the support or catalyst may lead to detachment of the catalyst [149,150]. Moreover, the corrosion of the support can also lead to the loss of active material [149,150].

4.2. Activity descriptors

In chemical reactions, catalysts reduce the activation energies. In the case of heterogeneous electrocatalysts, the catalyst must be conductive in order to allow the exchange of electrons from its bulk to the reaction center at its surface. Most commonly transition metal catalysts are employed as the electrocatalysts for the hydrogen evolution reaction (HER) and oxygen evolution reaction (OER) as they simultaneously show activity for the reactions and provide electric conductivity. The most active metals for these reactions can be found in the right half of the transition series of the periodic table [151], which is later ascribed to their electronic structure. The aim of following section is to give a general description of the working principle of electrocatalysts.

To catalytically promote a reaction, first the reactants have to be adsorbed on the catalyst surface. Adsorbed ions, atoms or molecules can diffuse along the surface of the catalyst and thereby meet other ions, atoms or molecules to react with [152]. Finally, when the product is formed it must be desorbed so that the reactants can bind on the surface of the catalyst again [152]. The adsorption strengths with the reactants, intermediates and products are determined by the electronic structure of the catalyst's surface [153,154] and finally determine the activation energy of the electrochemical reaction.

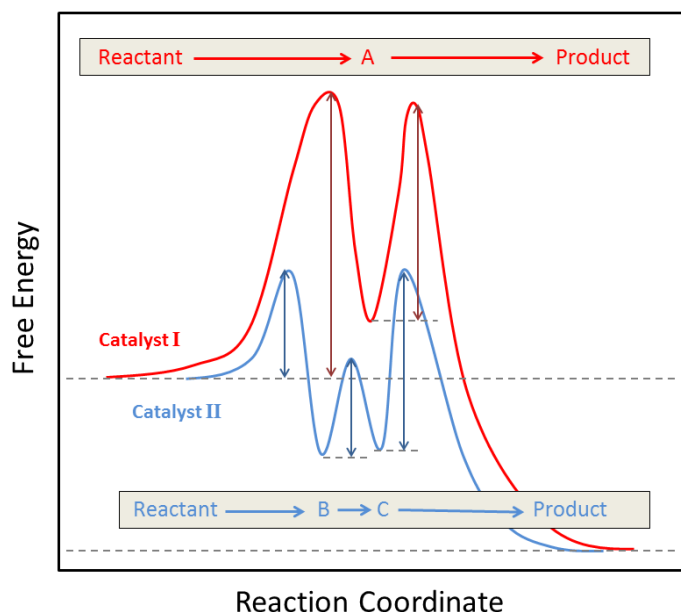


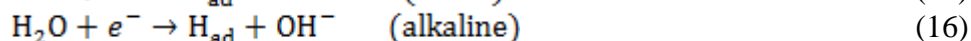
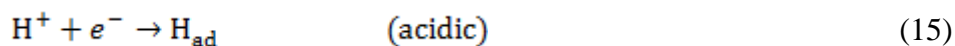
Figure 14. Schematic illustration of the free energy as a function of the reaction coordinate for a reaction with two different catalysts (red and blue) on the basis of reference [155]. The letters A, B, and C represent different intermediates that are adsorbed on the electrode. The ochery shaded boxes indicate the reaction equation with reference to the reaction coordinate. Vertical blue and red arrows: Activation barriers to overcome for the reaction steps.

Sabatier principles of catalysis says that the interaction strength between the catalyst surface and species that are involved in the reaction should be neither too strong nor too weak in order to yield high reaction rates. Figure 14 shows a schematic illustration of the free energy of the reaction as a function of the reaction coordinate for different catalysts. The catalyst reduces activation barriers and can also affect the reaction pathway. Each adsorbed species involved in the reaction has to overcome an individual activation energy in order to allow the overall reaction [152,155,156]. These individual activation energies depend on the adsorption strengths at the catalyst's surface [152,156]. The more adsorbates and intermediate reaction products are necessary for a reaction, the more difficult it is to develop a catalyst with optimized adsorption energies for all of these species. The reaction step that deviates the most from condition of thermoneutral adsorption finally limits the reaction rate [156]. The facet of the surface of the metal catalyst affects the adsorption strength and thus its activity, as for instance examined for the HER on platinum in detail [157,158].

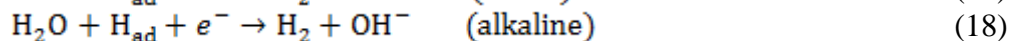
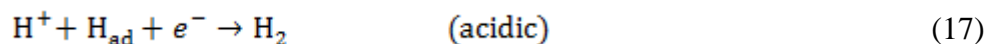
4.3. Hydrogen evolution reaction (HER)

During the HER, noble metal catalysts such as platinum are not passivated by amorphous oxide layers, for which these metals are model systems to experimentally study and to computationally model the nature of the electrocatalytic reaction mechanisms.

Reaction pathways - The first step of the HER is given by the so called Volmer reaction step, where a hydrogen atom is adsorbed on the catalyst. In the acidic and alkaline media this reaction step is displayed by:



The adsorbed hydrogen atoms can further react to hydrogen molecules as described by the Heyrovsky reaction step:



Alternatively, two hydrogen atoms adsorbed by the Vollmer reaction step can form a hydrogen molecule, described by the Tafel reaction step:



Effect of pH - The only intermediate of the acidic HER are adsorbed H atoms, while protons display the reactants and H_2 the product of the reaction. In the case of alkaline HER, water is the reactant and adsorbed H atoms are again intermediates. Some authors report that OH is an additional intermediate involved in the alkaline HER [159–163]. Accordingly, the alkaline HER potentially involves one intermediate more than the acidic HER. Several authors reported a decreasing activity of platinum (the best pure metal catalyst for the HER) with higher pH, which was attributed to a higher binding energy of hydroxide molecules than that of the hydrogen atoms [159–163]. At the same time some authors [159] disputed importance of OH adsorbed and attributed the lower reaction toward higher pH to the oxophilicity of the catalyst surface. Nevertheless, the trends for the activities of the HER across the periodic table in the alkaline and acidic regime are similar [164].

Adsorption - As discussed above, the free energy of adsorption is a decisive property for the rate of electrocatalytic reactions. Krishtalik [165] extracted the hydrogen adsorption strength on pure metal surfaces from electrochemical measurements. Different authors computed the hydrogen adsorption energy on metals using DFT calculations [166,167]. Figure 15 shows a comparison of measured bond strengths and computed hydrogen adsorption energies of noble metals, Ni and Co. Schmickler and Trassatti [168] proposed a linear relation of the computed and measured values. However, this trend is with reference to Figure 15 not obvious. Especially the values of Ni and Co do not follow this linear trend.

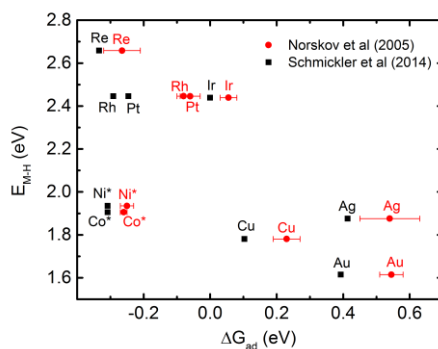


Figure 15. Comparison of measured values of the metal hydrogen bond E_{M-H} (reported by Krishtalik [165]) and computed values of the Gibb's energy of adsorption ΔG_{ad} (Norskov et al. and Schmickler et al. [166,167]). The errors bars of Norskov's data (in red) represent the upper and lower limit of the simulations with two different surface coverages. A similar comparison was previously reported by Schmickler and Trassatti [168].

Activities for the acidic HER: Volcano-type relation? - On the basis of Sabatier principles of catalysis, Balandin introduced in the 1920ties plots of the reaction rates as a function of adsorption energies of species that are involved in the reaction. These plots are of a volcano-type shape and are thus commonly referred to as volcano plots. Conway and Bockris [153] first reported such a volcano type relation for the work function of metals as a function of the strength of the metal hydrogen bond (which calculated on the basis of the simple Pauling Equation [169]). Parson developed a kinetic model that relates the reaction rate of the HER to the adsorption [154]. Trasatti [170] introduced the most commonly used depiction of a volcano plot for the HER that is graphed in Figure 16A, plotting the logarithmic exchange current density $\log(j_0)$ of the HER as a function of the metal hydrogen bond (with reference to the adsorption strengths measured by Krishtalik [165]).

In modern volcano plots as pioneered by Norskov et al. [166], the measured activities are related to the calculated free energy of adsorption ΔG_{ad} . Norskov et al. modeled a similar volcano shaped curve as that of Trasatti. DFT calculations of the free energy of adsorption for the non-noble metals (Mo, W, Nb, etc) were criticized, as these do not take into account their oxide coverage in aqueous solutions [167]. Accordingly, these oxide covered metals are not considered here. Schmickler et al. also developed a model for electrocatalysis of hydrogen evolution [171] which is based on a model Hamiltonian, quantum statistics and DFT. Figure 16B shows $\log(j_0)$ as a function of the free energies of adsorption that were modeled by Norskov and Schmickler et al. As described by Schmickler et al, $\log(j_0)$ is linearly related to adsorption energies when the oxide covered metals are not considered. In other words, when compared to Trasatti's experimental volcano (Figure 16A), the entire descending branch of volcano curve is missing.

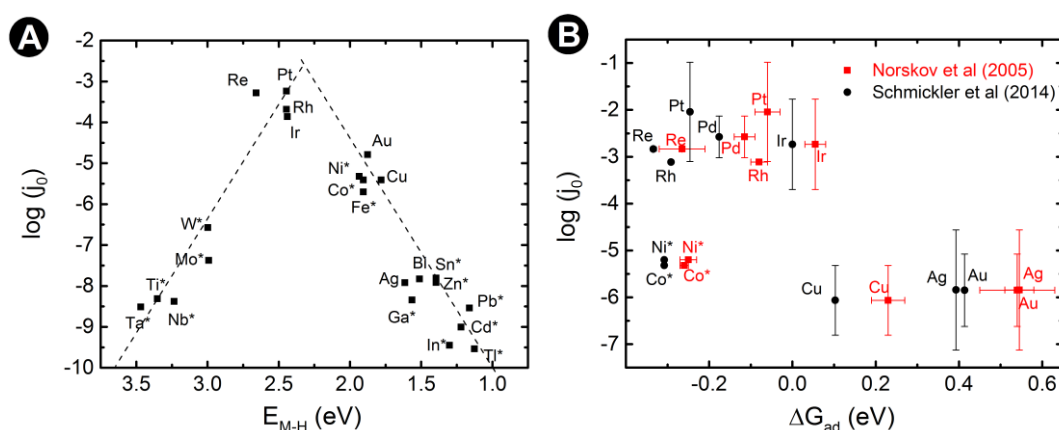


Figure 16. Different relations between exchange current for the hydrogen evolution reaction in acidic media and the bond strength of hydrogen: A) Trasatti in 1972, replotted from reference [170]. B) Computational data on the Gibb's free energy of the hydrogen adsorption by Norskov et al (graphed in red) in 2005 and Schmickler et al (graphed in black) in 2014, replotted from the references [166,167]. The errors bars of the logarithmic exchange current density represent the highest and lowest values that both authors reviewed from experiments reported in the literature. The errors bars of ΔG_{ad} calculated by Norskov et al. represent two different surface coverages.

Krishtalik's measured the hydrogen bond strength to the metals of the iron group (Fe, Ni and Co) to be relatively weak, while relatively strong hydrogen adsorption on Ni and Co was reported by computational studies (Figure 15). Lower activity of Ni and Co in comparison to the platinum group metals was attributed by Schmickler et al. to their more compact $3d$ -orbitals than the $4d$ and $5d$ orbitals and the resulting smaller overlaps with the orbitals of adsorbed hydrogen atoms. For further insights in electrocatalysis of HER readers are directed to a recent critical review [172]. To summarize, the mechanisms of the HER and adsorption strengths of intermediates are still debated, while different assumptions or approximations for DFT calculations lead in many cases to significant differences and inconsistencies.

Work function and activity - As pointed out in the latter paragraph, the relation of the metal-hydrogen bond-strength to the kinetics is still a disputed topic. Alternatively, direct correlations between the electronic structure of the metal catalyst and the activity for the HER were established by comparison of the work functions, electronegativities, and potential of zero charge of the metals with their catalytic activity [153,170,173,174]. Trasatti showed that the relation of Pauling's electronegativity, the work function, and the potential of zero charge to the logarithm of the current exchange density is of an approximately linear character [170]. Despite the link between work function and hydrogen-adsorption strength is not obvious, the work function may be the best measurable indicator for the catalytic property of pure metal catalysts.

4.4. Oxygen evolution reaction (OER)

In the OER twice the number of electrons and more intermediates are involved in comparison to the HER. Moreover, mixed stoichiometric oxides appear during the OER that result in amorphous oxide or passivation layers. In contrast to the HER, the oxygen involved in the OER can change the oxidation state of the catalyst and thus its overall electronic and crystallographic structure. A detailed computational modelling of the energy states during the reaction is thus difficult. DFT calculations that describe OER electrocatalysts are typically performed for idealized oxide crystals or clean metal surfaces [175–178]. Despite these differences between the modeled and real surfaces at OER catalysts, DFT calculations provide relevant insights to the reaction mechanisms during the OER. However, with respect to these uncertainties of the computation approaches to describe the OER, detailed correlations between the electronic structure and the activity will be not considered here. Instead, in this section a brief review on the mechanisms of the OER is presented. A more detailed analysis of the mechanisms during the OER are provided by several reviews in the recent literature [155,179–181].

Reaction pathways - The four electron process of the oxygen evolution is accompanied by at least 2 different intermediates, namely OH and O [126,182]. In addition, usually the participation of OOH is assumed [126,182], which however can be avoided when two adsorbed oxygen atoms are chemically recombined to an oxygen molecule. Oxygen - as the product of the reaction - is also adsorbed on the catalyst. In the alkaline regime, OH⁻ is the reactant while water is the reactant in the acidic regime. In both cases the reactants also have to be adsorbed on the catalyst in order to start the

reaction. Figure 17 illustrates different electrochemical pathways for the OER as reviewed by Giordano et al [183]. Despite the intermediate adsorbates OH, O and OOH for the OER in the alkaline and acidic regime are equal, the reaction rates of the different pathways sketched in Figure 17 can be influenced individually by pH. Giordano et al [183] showed that no general trend for the overvoltages (or the potential vs the reversible hydrogen electrode) as a function of the pH can be given.

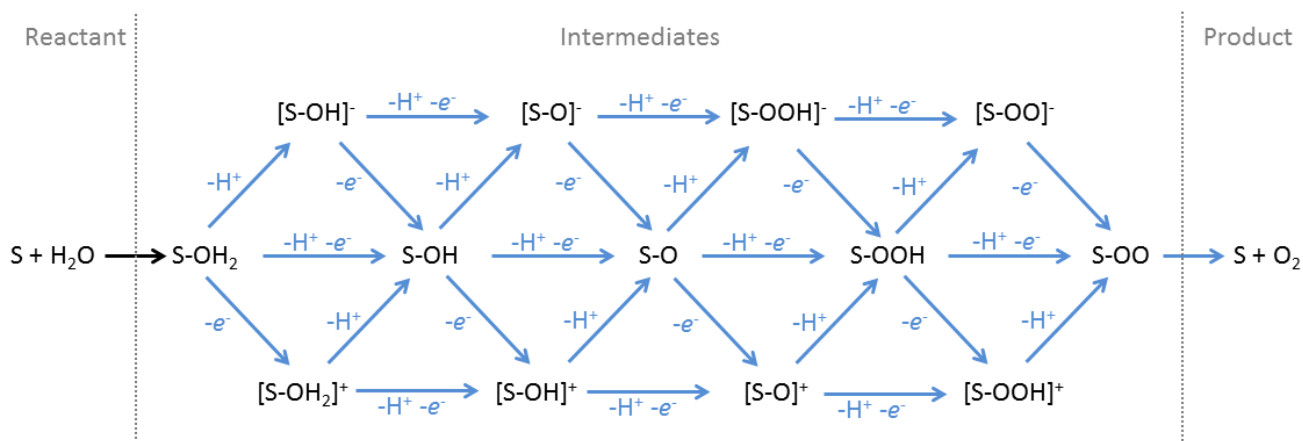


Figure 17. Reaction pathways of the OER adopted from Giordano et al [183].

Structure of OER catalysts - The potential region where the OER takes place is above the standard potential of all metals. Thus, metal catalysts must be protected by an oxide layer in order to avoid rapid dissolution. Alternatively, bulk metal oxides can be used as the catalysts. As discussed in Section 4.1, metal or metal oxide catalysts are not thermodynamically stable during the OER and thus their dissolution is just a question of kinetics. Moreover, the morphology of the hydrous amorphous oxidation layer undergoes constant changes during the OER. Accordingly, the surface of the electrocatalyst during the OER cannot be precisely defined and it is challenging to obtain physical information of the amorphous nature of the hydrous oxide layers. By using spectroscopic in-situ measurements, various oxidation states of the active metal components during the oxygen evolution were measured [102,126–131]. Although the reaction takes place at or in the amorphous surface layer, the activity and stability of the catalyst may also depend on the bulk properties. For instance, oxide covered Ru and Ir metals were observed to be more active but less stable than their bulk oxides [125].

Conductivity - Metals typically show conductivities of at least 10^4 S/cm. The conductivity of IrO_2 and RuO_2 is of a metallic character with similar high values [184], while other metal oxides typically show semiconducting or insulating behavior with conductivities that are orders of magnitude smaller. Trotochaud et al [185] measured the conductivity of pure NiOOH in the order of 0.1 mS/cm, while iron impurities increase the conductivity by more than an order of magnitude. Thus, the conductivities of such oxides are typically two to four orders of magnitude smaller than those of the employed electrolytes (Section 2). The conductivity of the electrocatalysts is especially relevant for the design of electrodes, as further discussed in Section 5.

4.5. Surface area

At structures in the nanometer scale, the surface atoms have due to geometric reasons on the average less binding partners compared to surface atoms at flat surfaces. Moreover, the electronic structure of the bulk also changes when the mean free path of electrons in a conductor is reduced [152]. Both effects are expected to increase the adsorption strength of ions/molecules and atoms of high surface area configurations compared to their plane counterpart [186]. For example, in comparison to polycrystalline flat metal electrodes a drastically lower surface-normalized activity of Ru, Ir, and Pt nanoparticles towards the OER was reported [187].

Besides the influence of the surface area on the electronic structure of an electrocatalyst, its precise surface area determination is crucial to precisely characterize the activity. Most commonly, the activities of electrocatalysts for the HER and OER are determined by measuring the current attributable to the HER or OER as a function of the potential of the catalyst in the electrolyte. The current ideally linearly correlates with the electrochemical active surface area (ECSA) of the active component or components of the catalyst. Thus, in order to characterize and compare the activity of different catalysts, the measured currents should be normalized to their ECSAs. Unfortunately, ECSAs are in many cases difficult to measure, which makes a comparison of different catalyst materials difficult.

Electrochemical methods to measure the ECSA of metal catalysts that were reported in the literature are based on the following physical properties [188]: (i) The double layer capacitance at the interface of the electrocatalyst to the electrolyte [189] is a measure for the surface area of a catalyst. Typically, the capacitance is measured via impedance [190,191] or by small excitations of triangular potential waves (cyclic voltammetry) [192,193]. (ii) Adsorption of gases (CO, H₂, O₂) [194–198] or ions in the electrolyte [199–202] on the surface of the catalyst, which are subsequently electrochemically converted. (iii) Voltammetric measurements, in which the oxidation state changes of the active component are measured [203].

The double layer capacitance measures the surface area of the catalyst and its support. Accordingly, for supported catalyst this method is generally not suitable for measuring the ECSA of the active component. Excitation amplitudes and frequencies (impedance) or scan rates (cyclic voltammetry) for capacitance measurements have to be chosen with great care, otherwise experimentally determined capacitances can be by orders magnitudes wrong [204]. Moreover, electrode capacitances can be individually affected by adsorption processes or side reactions [204,205]. Hence, capacitance measurement can be not considered as a generally appropriate technique to precisely determine surface areas of electrocatalysts. Carbon monoxide or hydrogen stripping can be considered as a very effective technique to measure the surface area of platinum group metals [195,206], while this technique is generally not applicable to other metals.

Besides electrochemical measurements, physical adsorption of gas molecules on the catalyst surface (as described by the Brunauer-Emmett-Teller (BET) theory [207]) is often used to measure the surface area of porous catalysts or powders [208]. Moreover, atomic-force microscopy (AFM) can be used in order to determine the roughness factor (and thus the ECSA) of thin film catalysts [209].

In a water electrolyzer, the ECSA of an electrode is a decisive property for its electrocatalytic performance. In the case of precious metal catalysts (for example Ir or Pt), high ratios of the catalyst surface areas to mass are aimed to reduce the amount of catalysts and thus costs. Dealloying is a common procedure to realize nanoporous catalysts with high surface areas [210–212]. Hereto, a catalyst is alloyed with a component that dissolves faster in a certain solution than the catalyst itself. After dealloying a porous stable skeleton of the catalyst should ideally be left. Nanostructures also can be obtained by direct synthesis [213] of (i) nanoparticles [186], (ii) core-shell structures [214], (iii) hollow spheres [215], (iv) nano architectures (such as dendrites [216], nanowires [217], nano-frames [218], nano-cages [219], etc), (v) single-molecule active sides [220] or (vi) electrodeposition of porous films [221,222]. However, the long-time stability of filigree nanostructures is especially towards the OER questionable [223].

4.6. Composite and alloy electrocatalysts

At composite or alloy electrocatalysts different synergetic effects may occur, as graphed in Figure 18: (a) The electronic environment around an active component can be altered by the interaction of different elements and thereby the adsorption strength can be optimized. The activity towards the HER or OER can thus be improved [224]. (b) When a species involved in the reaction bonds simultaneously to different surface atoms of the catalyst, the adsorption energies can be tuned by employing different active sites [209]. (c) Adsorbed species can diffuse on the surface of the catalyst [225–228]. Thus, in a composite electrode adsorbed species can diffuse from one active component on the metal surface to another. When the adsorption energies for two different species involved in the reaction are at different active sites favorable, diffusion between the different atoms at different reactions steps can increase the overall activity.

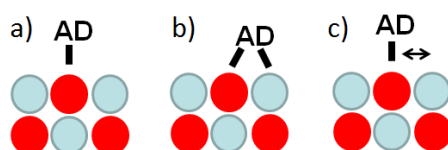


Figure 18. Schematic sketch of an adsorbed species (AD) on a composite interface, that consist of two different elements as graphed in red and blue. (a): The adsorbate bonds to one surface atom, while the electronic structure is changed by alloying and thus affects the bond strength. (b): The adsorbate bonds to at least two different surface atoms and thus the adsorption strength is different from the bonding to the single surface atoms, respectively. (c): Diffusion of adsorbates diffuse between different atoms on the surface, so that at different reaction steps the bonding strength is varied.

Different or no surface normalization of reported activities in the literature makes the comparison of reported data on alloy catalysts difficult. For example, in the case of Ni-Mo alloys strongly deviating results for activities towards the HER were reported [229–232]. From a theoretical perspective, an alteration of the *d*-band structure was predicted to yield high activities of Ni-Mo alloys

[233–236]. However, recently the activities of plane Ni-Mo alloy electrodes were reported to equal that of plane Ni electrode [205]. In this study, different activities of Ni-Mo electrodes reported were attributed to different porosities and roughness factors that come from different fabrication procedures.

In general, reported activities of rough or porous samples must be considered with care, as it is often difficult to distinguish between the effect of surface area and electronic structure on measured potential-current curves. A difficulty to calculate binding energies of composite catalysts is displayed by partial oxide/hydroxide coverage and a related amorphization of the surface. During the OER, the discussed amorphization of the surface rearranges the defined crystal structures of alloys or the initial morphology of composites. Accordingly, it is questionable, whether different elements can passivate one another during the OER, if they do not show stability on their own.

4.7. Electrocatalysts in water electrolyzers

In the following, electrocatalysts suitable for the anode and cathode in water electrolyzers are elucidated. As discussed above, the activities of pure metals in the form of the current exchange density for the HER were reported. The platinum group metals (PGMs) show the best activity for the HER, followed by Ni and Co. In acidic electrolyte, Ni and Co based catalysts were reported to be unstable [237], for which platinum metals are typically used in acidic water electrolyzers for the HER. In alkaline electrolytes, the PGMs also show the highest activity for the HER [167] while Ni and Co based catalysts are stable.

In the case of the OER, dissolution and high resistances are major disqualifiers for many metals or metal oxides. In Figure 12, the thermodynamic stability and abundance of metals across the periodic table was graphed. The metals Ir, Pt, Pd, Rh, Ti, Ta, Nb, W and Si show a thermodynamically stable oxide phase at the potentials that occur during the OER. The oxides of the metals of the early transition series and Si however show low conductivity and low activity towards the OER. Of the mentioned metals, Ir shows the highest activity towards the oxygen evolution reaction [121] and is therefore most frequently used as OER catalyst. Another advantage of Ir is that its oxide IrO_2 shows high conductivity [184]. However, the scarce Ir and the costs for the other platinum metals might display a bottleneck when aiming at large scale water electrolysis with acidic electrolytes.

In alkaline electrolyte, most PGMs show higher dissolution during the OER compared to acidic electrolytes [121,122]. However, a measureable dissolution of Ni, Co and Fe could not be observed [125]. Using these metals as active components for alkaline OER catalysts, a broad class of metals and oxides with different structures (such as perovskites, spinels, rutiles, etc) were reported, as extensively reviewed in the literature [155,180,238]. However, partial dissolution and amorphization of the surface of perovskites was observed [239,240], which may display an issue of such defined crystal structures. In the case of Ni metal anodes, small amounts of anodically deposited or incorporated iron oxides from iron impurities in the electrolyte were reported to significantly increase the activity for the OER [185,241–245]. In order to avoid conductivity issues with Ni, Co or Fe based electrodes, rather passivated metal electrodes than bulk oxides are typically used. The amount of these metals in the earth crust is almost four orders of magnitude larger than that of the platinum metal group (Figure 12).

Hence, the amount of these metals for the use as electrocatalysts in alkaline electrolyzers is not limited by the costs.

Catalysts on the basis of nitrogen doped carbon were initially reported for the oxygen reduction reaction in fuel cells [246] and later also suggested to be suitable to catalyze the OER [247]. Moreover, carbon based structures were discussed as the support of metal catalysts for the OER [248,249]. However, the low stability of carbon at elevated temperatures and high anodic potentials during industrial water electrolysis is expected to display an issue for the durability of these carbon based or carbon supported catalysts. In contrast, at the cathodic potentials during the HER, carbon is stable and thus can be used as support for catalysts.

4.8. Section summary

In this section, first the stability of metals in alkaline and acidic electrolytes and mechanisms for their dissolution are reviewed in order to identify materials that can be used as electrocatalysts for water electrolysis. Next, the mechanisms for the HER and OER are elucidated, showing discrepancies and open questions. Towards application, reasonable electrocatalysts for water electrolyzers are discussed. In alkaline electrolyte, the abundant and cheap metals of the iron group (Fe, Co and Ni) are active and stable electrocatalysts for the HER and OER. Iridium displays the catalysts with the best activity and stability compromise for the OER in acidic water electrolyzers, while the HER can be efficiently conducted with all platinum group metals. The amount of these noble metals usable in the electrodes is restricted to their low abundance and the resulting high costs.

5. ELECTRODES, CURRENT COLLECTORS AND BIPOLAR PLATES

5.1. Electrodes

As discussed in Section 2, typically metal electrodes are used in alkaline water electrolyzers that consist of a porous metal framework (mesh, perforated metal, foam, sintered bodies, etc.) and high surface area catalyst coatings. In the case of PEM water electrolyzers, composite electrodes consisting of polymer electrolyte binder and catalyst nanoparticles (which can be attached to conducting supports) realize porous structures.

Design factors - To enable an electrochemical reaction at an electrocatalyst, it must be in contact with an electron conducting solid phase and an ion conducting phase. The electron conducting solid phase can be composed of metals, metal oxides or carbon [250]. In the electrodes of PEM water electrolyzers, the polymer electrolyte provides the charge carriers (protons or hydroxide ions) that dissolve in the aqueous phase and thus provide the ionic conductivity [251,252]. Liquid electrolytes can penetrate into porous electrode structures and thereby also provide the ionic conductivity. The production of hydrogen and oxygen leads to gaseous phases at the electrocatalysts. The simultaneous

occurrence of the solid, aqueous and gaseous phase at the catalysts is commonly referred to as triple phase boundary [253].

Bubbles that are attached to the surface of the catalyst reduce the area of the liquid-solid interface [254–256]. Besides the blockage of the catalyst, gas bubbles also can block pores through which proton or hydroxide ion conduction takes place. Accordingly, fast transport of the evolved bubbles from the electrocatalyst to the surrounding is a decisive property of an electrode, which is typically realized by porous structures. At atmospheric pressure, the gases evolved have more than 1000 times higher volumes per mass as water (as calculated by the ideal gas law). As a consequence, the pressure inside the electrode increases by the phase transition of the liquid reactants to the gaseous products. The resulting differential pressure between the inside and the outside of the electrode was estimated to display the dominating driving force for the gas transport through the electrode, while the contributions of diffusion to the overall gas transport were estimated to play a minor role [27]. The gas flux from the inside of the porous electrodes through its pores to the bipolar plate or the current collector convectively carries the electrolyte or water through the porous electrodes. By capillary pressure, the aqueous phase can penetrate into the pores of the electrode again.

Smaller pores of the electrodes increase the friction of the electrolyte and gas transport and thereby increase the pressure drop that is caused by the gas transport. However, smaller pores can increase the surface area of the catalysts and the capillary pressure. An electrode ideally shows following macroscopic properties:

- High conductivity to electrons and ions in order to minimize Ohmic drops.
- High wettability so that the catalyst is in contact with the aqueous phase.
- High surface area of the catalyst.
- Low bubble coverage of the catalyst and a low amount of bubble-blocked pores.
- High permeability to gases and electrolyte in order to ease mass transport.

In the following, strategies to realize such structures are discussed.

Electrodes with polymer electrolytes - The electrodes of SPE water electrolyzers typically consist of mixtures of polymer electrolytes and high surface area electrocatalysts in the form of nano-architectures [257,258]. At low catalyst loadings, the volume fraction of the electron conducting phase decreases. As a result, less catalyst particles touch one other and so a reduced macroscopic electron conductivity of the catalyst layer results. Supports for the catalysts (such as graphite for the cathodic catalyst [259–261] and tin oxide [262] or titanium oxide [263,264] for the anodic catalyst) can be used in order to increase the electric conductivity and/or mechanical stability at low catalyst loadings. However, as discussed in Section 4.4., except IrO₂ and RuO₂ oxides are typically poorly conducting, for which suitable anodic catalyst supports are still to be developed. The polymer electrolyte binder in the electrodes provides the ionic conductivity [251,252], enables water uptake [265] and mechanically fixes the catalyst powders.

Electron tomography was used to characterize the morphology of the different phases (catalyst, support and electrolyte) in detail [266,267]. In these studies pore diameters that were one or two orders of magnitude larger than those of Nafion membranes (which were reported to 2.5nm [53]) were reported. These larger pore diameters of the catalyst layers enable larger differential pressure

permeability than that of the Nafion membranes. The best performance of catalyst layers in PEM water electrolyzers is typically obtained with Nafion loading in the range from 20 wt% and 30 wt% [257]. The composite electrodes are produced analogously to that of PEM fuel cells [268–274].

Solid electrodes for liquid electrolytes – Electrodes for alkaline water electrolysis with liquid electrolytes typically consist of porous metal frameworks (that provide high electric conductivity) covered with high surface area catalyst layers [275,276]. The metal framework typically consists of nickel, which is cheap and chemically stable in the alkaline regime. Alternatively, porous metal foils can be directly obtained by dealloying [209,277], which however might display a lack of permeability to differential pressures and thus might be problematic concerning the gas transport.

Following structures are typically used to realize metal frameworks for the electrodes: (i) Solid meshes [275,276,278], which can be prepared by weaving or acid leaching. (ii) Perforated metal plates [27], which can be produced by melting of metal fabrics, acid leaching, or drilling. (iii) Powder electrodes [279], which are fabricated by sintering of metal powders [280,281]. (iv) Metal foams, which can for example be fabricated by deposition of a metal into a porous structure which is subsequently leached out [282,283]. (v) Porous metal foils, which can be produced by tape casting of an oxide which is subsequently reduced at high temperatures [284].

Common coating techniques to put catalyst coatings onto metal templates are: (i) Vapor plasma spraying, where a metal plasma is sprayed onto the template [275,276,285]. (ii) Chemical and physical vapor deposition [286], in which thin catalyst layers can be deposited onto the substrate. (iii) Electrodeposition, where metals are cathodically deposited on the metal framework. Porosity can be obtained directly by the deposition procedure, for example by gas evolution during deposition [230,287–290]. (iv) Electroless deposition in an electrolyte [291–293]. For the latter two wet chemistry approaches a variety of techniques to deposit Ni-based alloys with non-metals such as phosphorus [294,295], Sulfur [293], Boron [292,296] and metals such as Molybdenum [230,289,290], Zink [297], Copper [298], etc. were reported. The deposition in non-aqueous electrolytes can broaden the amount of metals which can be deposited [299].

5.2. Current collectors and bipolar plates

The electric conductivities of metals are typically with at least 10^4 S/cm more than four orders of magnitude higher than the ionic conductivities of electrolytes (Section 3). Thus, the Ohmic drops in the current collectors and bipolar plates of water electrolyzers typically display minor contributions to the overall Ohmic drop in electrolysis cells [27]. However, at the interface between the electrodes, current collectors and bipolar plates, where less conducting passivation layers occur, significant electric resistances can occur (Section 4.4). Moreover, at these interfaces contact resistances can lead to significant contributions to cell resistance [27].

Acidic water electrolyzers - In PEM water electrolyzers, current collectors are used to contact the composite electrodes and to compensate their weak in-plane conductivity [250]. Moreover, the

current collectors mechanically support the PEM. The current collectors are in direct contact with the catalyst layers and are thus at least partly exposed to their corrosive acidic aqueous phase. The bipolar plates in acidic water electrolyzers are not in contact with the corrosive aqueous phase of the PEM. However, when PFSA membranes such as Nafion are used, hydrogen fluoride can be formed by the degradation of the membrane [58,300]. The hydrogen fluoride produced by the membrane degradation permeates into the water supply and leads to its acidification. The acidic solution containing fluoride in combination with the high anodic potentials display a harsh environment for the metals used as current collectors and bipolar plates. When metal cations are dissolved from the current collector or bipolar plate, these can penetrate into the polymer electrolyte and replace the protons of the functional group and result in a loss of the conductivity of the SPE [301]. Moreover, transition metal ions in the membrane can accelerate its degradation [302]. Thus, the stability of the bipolar plate and the current collector is of significant importance for the overall durability of SPE water electrolyzers.

In the acidic regime, only a few metals are stable at potential during the OER (see Section 4.1). Titanium is the cheapest material that displays a stable and (at least poorly) semiconducting oxide [303] in the acidic regime with respect to the anodic potentials applied. However, its passivation layer continuously grows and thereby increase contact resistances. The anodic current collectors are typically made of titanium meshes or sintered bodies of titanium spheres [304]. In order to avoid the formation of thick and bad conducting passivation layers, precious metal coatings can be used for the titanium-based bipolar plates and current collectors [305]. Carbon can be used as a stable material with low contact resistances for cathodic current collectors and bipolar plates. The contact resistances between carbon fleeces or papers and the current collector are in the order of $8 \text{ m}\Omega \text{ cm}^2$ [306], which is a negligible contribution to the overall cell resistance [27]. A further advantage of the porous carbon materials is their flexibility that provides uniform contacting of the electrodes [307,308] and that can balance thickness variations of the bipolar plates, catalyst coated membranes and anodic current collectors.

Alkaline water electrolyzers - In alkaline water electrolyzers, electrodes with a conductive metal framework realize high in-plane conductivity. Hence, current collectors are in alkaline water electrolyzers typically not employed as the porous metal frameworks of the electrodes adopt their functions. The electrodes can be directly pressed or welded onto the bipolar plates. By welding of the electrodes to the bipolar plates contact resistances between both components can be avoided. Typically nickel bipolar plates and current collectors are employed, as nickel is cheap, abundant, stable and shows low contact resistances.

6. CELL PROPERTIES

A detailed analysis and description of the cell properties in the form of voltage-current characteristic, heat balance, gas purities and efficiency is described in a previous study [27]. In this section, the most important aspects and relations of the cell properties to the previously discussed physicochemical material properties are highlighted.

6.1. Voltage-current characteristic

The voltage-current characteristic of a water electrolysis cell describes the relation between cell voltage and cell current and is a measure for its electrochemical performance. The cell voltage equals the sum of the Nernst voltage U_N , kinetic overpotentials U_{kin} , Ohmic drops U_{Ω} , and overpotentials related to mass transport phenomena U_{mass} [27]:

$$U_{cell} = U_N + R_{cell} j + U_{kin} + U_{mass} \quad (20)$$

The Ohmic drops of different cell components is analyzed in the literature in detail [27]. When the evolved bubbles cover the surface of the catalyst and thus block the access of liquid water, reactant starvation can result which leads to an exponential increase of the cell voltage with the current density [24]. However, this effect was not observed at current densities below 2 A cm^{-2} in state-of-the-art alkaline and acidic water electrolysis cells [27] and thus is not considered here. Figure 19 illustrates a typical UI-characteristic of a water electrolyzer. The partial pressure increase in the electrodes caused by the gas transport increase the Nernst voltage with current density [27].

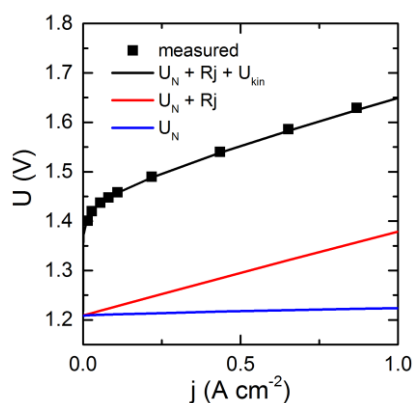


Figure 19. Typical UI-characteristic of a water electrolyzer including the Nernst voltage, Ohmic losses, and kinetic losses. Modeled data (lines) and measurements (scatter) of an acidic water electrolysis cell with a Nafion 112 membrane replotted from reference [27].

6.2. Heat balance

The heat balance of a water electrolyzer is influenced by the following factors [309]:

- The overpotentials caused by the Ohmic and kinetic losses that heat the cells.
- The amount of water vapor in the produced gases.
- Heat dissipation into the environment.
- The energy required to heat the water supplied to the same temperature as the cell.
- Recombination of hydrogen and oxygen in the cell.

LeRoy et al. [309] examined and described the influence of the first four points in detail, as in the following briefly reviewed. The heat dissipation into the environment is here not considered as this effect crucially depends on the design of the electrolyzer and the thermal insulation used. The temperature, at which the cell is in thermal equilibrium (temperature of the cell is constant without

active heat management) is typically defined as the thermal-balanced voltage U_{tb} (not to be confused with the thermoneutral voltage). Applying lower voltages than the thermal-balanced voltage ($U_{cell} < U_{tb}$) means that the cell temperature decreases until a lower equilibrium temperature is reached. Alternatively, additional heating can be supplied in order to maintain the temperature of the electrolyzer cell. With $U_{cell} = U_{tb}$ the temperature of the cell is constant, while higher voltages produce heat which increases the cell temperature or which must be carried away by the electrolyte flux that is purged through cell.

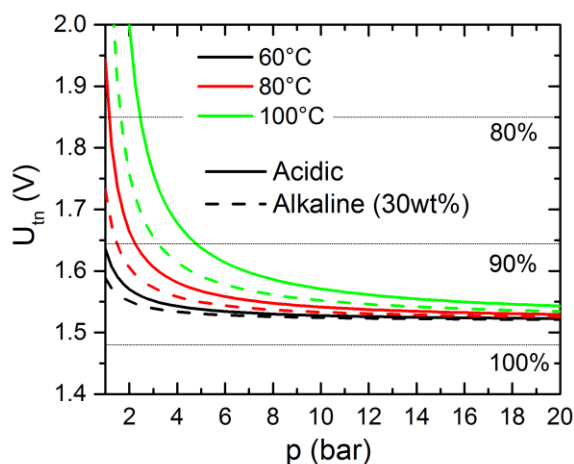


Figure 20. Thermal-balanced voltage as a function of the pressures applied to the anodic and cathodic compartment. Horizontal gray lines: Voltage efficiencies (normalized to the HHV). Calculated with reference to the equation reported in [27].

Figure 20 shows the thermal-balanced voltage as a function of applied pressure for different temperatures on the basis of the equation reported by LeRoy [27,309]. The absolute pressure negligibly influences the saturated vapor water pressure [310]. Accordingly, towards higher operating pressures the partial pressures of hydrogen and oxygen linearly increase but the saturated vapor pressure remains constant. As a result, the molar content of water vapor in the product gases decreases with higher pressures. Thus, the thermal-balanced voltage decreases toward higher pressures. At differential pressure operation with reduced anodic pressure (which can be realized with gastight SPE membranes), the increased mole fraction of water vapor in the anodic gas leads to a higher thermal-balanced voltage than at balanced pressure operation. In SPE water electrolyzers, which are fed with pure water, the saturated water vapor pressure is higher than in electrolyzers with alkaline electrolytes [311]. To summarize, pressurized operation is necessary to enable efficient operation in a voltage range from 1.5V to 1.7V at high temperatures without additional heat input.

6.3. Gas purities and pressurized operation

As discussed in Section 3, hydrogen and oxygen can diffuse through the separator/membrane in a water electrolyzer. Moreover, differential pressure forced electrolyte and gas permeation through porous separators significantly affects the gas purities. Mixing of hydrogen and oxygen in the anodic

and cathodic is commonly referred to as gas crossover. Generally, the gas crossover increases towards higher pressures. In a recent study [27], pressures of a few bars were motivated to yield the best compromise between moderate gas crossover and small thermal-balanced voltages. Hydrogen permeating from the cathode to the anode is typically not reacted at the oxide covered anodic catalyst [330] and thus mixes with the oxygen produced. In contrast, oxygen that permeates from the anode to the cathode can be electrochemically reduced at the cathodic catalyst. The gas purities typically increase toward higher membrane thicknesses and higher current densities [27].

Gas crossover equals an efficiency loss, as the separation of both gases (for example by liquefaction processes) is typically considered to be too energy intensive. In the case of high operating pressures, the gas crossover during pressurized water electrolysis can lead to explosive gas mixtures (more than 4% of hydrogen in oxygen or vice versa [312]). In this case, safety hazards related to these gas impurities may display a disadvantage of pressurized water electrolysis [313].

6.4. Cell efficiency

In the following, the cell efficiency of water electrolysis is described, which does not include the energy consumption of system components such as pumps or gas driers. Typically, the impact of the voltage-current characteristic and the gas crossover on the cell efficiency are considered separately, described by the voltage efficiency η_U and the current efficiency η_C . The cell efficiency η_{cell} equals the product of voltage and current efficiency:

$$\eta_{\text{cell}} = \eta_U \eta_C \quad (21)$$

The voltage efficiency equals the ratio of a reference voltage U_{ref} (the voltage related to Gibb's free energy or the enthalpy) to the cell voltage:

$$\eta_U = \frac{U_{\text{ref}}}{U_{\text{cell}}} \quad (22)$$

Normalizing to the reversible voltage (related to Gibb's free energy) means that the latent heat of the phase transition from liquid water to the gaseous hydrogen and oxygen is not considered. When the efficiency is normalized to the voltage that is related to the enthalpy, the energy that must be spend for the phase transition of liquid water to the gaseous hydrogen and oxygen is included.

The conversion efficiency of the HER and OER during water electrolysis is typically 100% under stationary conditions [193]. Moreover, parasitic electric currents between the anode and cathode of electrolysis cells are typically negligible, as the separator/membrane should be electrically insulating. In a stack, where cells are connected in series, parasitic currents between the cells through the water feed can occur [314], which is especially an issue of alkaline water electrolyzers where the water feed in the form of the alkaline electrolyte shows high ionic conductivity. However, these parasitic currents can be reduced to a negligible amount by a proper design of the stack [314]. Accordingly, gas crossover typically displays the dominating impact on the current efficiency.

A crucial parameter for the cell efficiency is the thickness of the separator/membrane. The Ohmic drop at the separator/membrane is proportional to its thickness (Ohm's law), while the gas cross-permeation fluxes scale with its reciprocal thickness (Fick's law and Darcy's law). Thus, the thickness of the separator determines the Ohmic drop and the gas crossover. Hence, the separator

thickness is decisive for both, the current and voltage efficiency. State-of-the-art efficiencies of acidic SPE and alkaline electrolyzers are discussed in the literature [27]. This comparison revealed, that the voltage efficiencies of both systems are approximately equal if similar separator/membrane thicknesses are used.

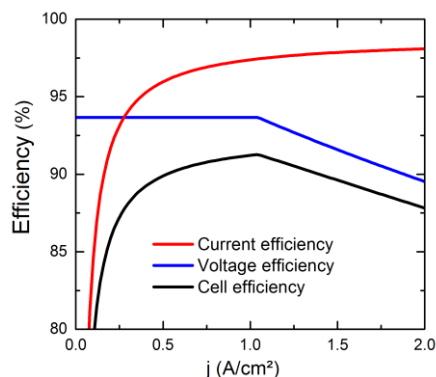


Figure 21. Voltage, current and cell efficiency (calculated on the basis of experimental data and normalized to the higher heating value) for an acidic water electrolyzer with a 50 μm Nafion membrane operating at 80 $^{\circ}\text{C}$, 6 bar cathodic and 2 bar anodic pressure. Data replotted from reference [27].

Figure 21 exemplarily shows the modeled efficiency of an electrolyzer as a function of the current density, with respect to an acidic water electrolyzer with a 50 μm Nafion membrane operating at 80 $^{\circ}\text{C}$, 6 bar cathodic pressure, and 2 bar anodic pressure. With this set of parameters a thermal-balanced voltage of 1.58 V results. Below current densities of 1 A/cm², this thermal-balanced voltage limits the voltage efficiency. Towards higher current densities activation and Ohmic losses increase, that finally reduce the voltage efficiency. The amount of the gases produced at the electrodes (Faraday's law) increase with the current density, so that the amount of cross-permeating gases in relation to the produced gases decreases. As a result, the current efficiency increases towards higher current densities.

6.5. Durability

Not many data for the long term operation of water electrolyzers in the order of at least 10,000 h are reported in the literature. Nevertheless, in the following we try to emphasize the physicochemical degradation mechanisms of water electrolysis cells on the basis of reported studies.

PEM electrolysis - In the case of acidic SPEs, the replacement of protons of the functional groups by other ions such as alkali metal ions results in a loss of conductivity [315]. SPE membranes can float under heat and pressure and thus lose their initial dimensional properties [96–99]. This phenomena was characterized for the operation conditions of fuel cells (SPE in contact with water vapor), however we could not find literature where this behavior was examined for water electrolyzers conditions (SPE is in contact with liquid water). The gas crossover and the resulting simultaneous

appearance of hydrogen and oxygen at the catalyst can lead to the chemical production of radicals such as HO[•], HOO[•] or H[•] [316–320] that can decompose the SPE [321]. In the case of fluorinated SPEs, hydrogen fluoride is one of the major degradation products [57]. The hydrogen fluoride can permeate into the supply water, reduce its pH and can lead to serious degradation of the cell components such as the current collectors and bipolar plates. Stucki et al [56] observed membrane failure in industrial water electrolysis stacks after 15.000h hours as indicated by a rapid increase of anodic hydrogen. Millet et al reported the end of life of a water electrolysis stack after 5500h due to membrane failure [322].

Serious degradation of the anodic iridium oxide catalyst in water electrolyzers was reported [323]. Due to high costs, only low amounts of the iridium can be used for industrial purposes. Thus, iridium dissolution during OER [125,324] may display a general issue for the service time of acidic water electrolyzers. When titanium is used as the base material for the bipolar plate and anodic current collector, its oxidation and the growth of a low conductive passivation layer can increase the Ohmic losses [325], which can be avoided by precious-metal coatings. However, precious metal coatings are expensive and could display an economical drawback of PEM water electrolyzers [326]. A more detailed review on PEM water electrolyzer degradation is provided by reference [327].

Alkaline electrolysis - The state of the art composite porous separators of Zirconium dioxide and polysulfone (denoted as Zirfon-type) may degrade during alkaline water electrolysis, as Zirconium dioxide can be dissolved in highly alkaline solutions. Pourbaix et al. [114] reported that at pH = 14 a concentration of 10⁻⁴ mole per liter of Zirconium ions is soluble. The Zirconium ions in the electrolyte cannot be deposited at the applied electrode potentials during water electrolysis. Thus, when the saturation concentration of Zirconium ions is reached in the electrolyte, the dissolution of the Zirconium dioxide particles in the porous separator is expected to stop (KOH-electrolyte typically not exchanged during operation). Schiller et al [275] showed 14.000h of intermittent operation of alkaline water electrolysis cells with nickel based electrodes and a porous Zirfon-type separator. The cell voltage dropped while no remarkable degradation of the cell or its components could be observed. At nickel cathodes or nickel bipolar plates, the formation of nickel hydrides [328] and hydrogen embrittlement [143,145] can display a source of degradation for the long-term operation. However, we could not find long-term data that show such effects in detail.

Degradation during standby - The stability of metals in acidic and alkaline electrolyte depends on the electrode potentials (Section 4.1). During standby, the discharge of electrode capacities and the adsorption of cross-permeated hydrogen/oxygen on the catalysts can reduce the cell voltage. Moreover, in stacks, the connection of different cells by the water/electrolyte supply can lead to large potential differences between the electrodes of the different cells. In the case of acidic water electrolyzers, the cathodic catalyst made of Pt/C can readily dissolve at potentials above 0.8 V as examined for fuel cell catalysts in detail [124]. The reduction and re-oxidation of anodic Ir based catalysts in the potential range from 0 to 0.8 V can also lead to severe dissolution [121]. In alkaline water electrolyzers, Ni is expected to dissolve when the electrode potentials are in the potential window between 0 V and 1.23 V (Figure 11). To avoid the drop of the cell voltage during standby and

the resulting dissolution, a cell voltage slightly higher than the Nernst voltage can be applied, for which a low amount of power is necessary.

6.6. Section summary

In this section, the interplay of operation parameters and the material properties on the cell characteristics such as the current characteristic, gas crossover and efficiency are discussed. Moreover, the effect of the applied pressures on the water content of the produced gases and its implications for the heat balance is reviewed. In general, toward higher current density the current efficiency increases while the voltage efficiency decreases. The reported data on the degradation of water electrolysis cells are reviewed. In the case of acidic water electrolysis, the degradation of the SPE, the dissolution of the anodic Ir based catalyst and bad conducting passivation layers in the anodic compartment may display serious issues for enabling long service life. In contrast, alkaline cells are expected to show higher durability, while the formation of hydrides and hydrogen embrittlement at the cathode may finally limit the service life.

7. MAJOR TECHNICAL CHALLENGES

On the basis of the discussed properties, following major technical challenges to improve acidic water electrolysis with SPEs were identified:

- More thermomechanical and chemical durable SPE membranes are necessary in order to achieve long service life.
- The amount of available iridium can display a bottleneck to meet the requirements of large scale industrial water electrolysis. Despite of intensive research activities on new catalyst for the acidic OER in the last decades, a suitable alternative to iridium was thus far not developed. With reference to the amorphization of catalysts during the OER, mainly the properties of the elements are expected to be responsible for electrochemical stability of anode catalysts. Accordingly, it is questionable, if other suitable catalysts materials than Ir can be physically stable for the conditions at the anode during water electrolysis.
- Corrosion and the low conductivity of passivation layers lead to degradation of bipolar plates and anodic current collectors. Using costly coatings with platinum group metals this degradation can be reduced, which displays however a major economical drawback.
- Lower hydrogen and oxygen diffusivities of the solid phase of SPE membranes may significantly reduce the gas crossover and thereby increase efficiency and ability towards high pressure operation.

Following challenges to improve water electrolysis with alkaline electrolytes were identified:

- Porous high surface area electrodes with efficient electrocatalysts must be developed in order to achieve low overvoltages. Hereto, the optimization of porous alloy catalysts with Ni, Fe or Co as active components could display a promising pathway.
- Hydride formation and hydrogen embrittlement of cathodic Ni-based materials may affect the

long-term stability. By alloy design, these drawbacks might be avoidable.

- Alkaline polymer electrolyte membranes or porous separators with small pores below 100 nm should be developed to reduce the electrolyte cross-permeation and thereby improve gas purities.

As state-of-the-art alkaline and acidic low-temperature water electrolyzers both achieve comparable performance [27], durability issues and costs for production display the major drawbacks of both technologies. In the case of large scale energy conversion by water electrolysis for renewable energy conversion and storage, alkaline water electrolysis might be more suitable than acidic water electrolysis, as the alkaline technology is not limited to the usage of scarce and precious metals for the catalysts and system components. Besides, alkaline water electrolyzers thus far showed higher durability which can be attributed to the different corrosion mechanisms in acidic and alkaline electrolyte. Finally, a chemically stable and exchangeable electrolyte is used in alkaline water electrolyzers, while SPEs for acidic water electrolyzers are vulnerable to a conductivity loss by impurities of the supplied water, chemical decomposition and thermomechanical deformation.

8. SUMMARY

This perspective aims to give an interdisciplinary, coherent and comprehensive overview of electrolytes, corrosion, electrocatalysis, component design, operation strategies and materials for low-temperature water electrolysis. Acidic and alkaline electrolytes are compared regarding their ionic conductivities, gas diffusivities and gas permeabilities. Acidic solid polymer electrolytes (SPEs) or liquid bases in combination with porous separators are discussed as suitable electrolytes for technical water electrolysis. The ionic conductivities of both electrolytes are similar, while the lower hydrogen and oxygen diffusivities in alkaline solutions in comparison to those in acidic SPE membranes display advantages of alkaline electrolytes. However, state-of-the-art porous separators in alkaline electrolyzers are more permeable to differential pressures than SPE membranes as their pore sizes are larger.

Corrosion mechanisms are reviewed and suitable metals for the use in water electrolyzers are discussed. Non-noble metals such as Ni and Co display reliable electrocatalysts for the hydrogen evolution reaction in alkaline electrolytes, while in acidic media their stability is a serious issue for which platinum group metals are typically employed. Currently, Ir and its oxides display as moderately stable and simultaneously active the best electrocatalysts for the OER in acidic electrolytes, while in alkaline electrolytes Ni, Co and Fe based catalysts are stable and active. Thus, acidic water electrolysis currently depends on precious metals as electrocatalysts and coatings for current collectors and bipolar plates. Reported theories that describe the hydrogen and oxygen evolution reaction were critically elucidated and related to the survey of suitable electrocatalysts.

The impact of material properties on the design of electrodes, current collectors and bipolar plates is discussed. The voltage-current characteristic, gas purities, heat balance and cell efficiency are related to operation parameters (such as current density, pressures and temperature). Durability challenges are reviewed, showing that the degradation of the SPE, the anodic Ir based catalyst and the

anodic current collectors of acidic water electrolyzers displays a crucial limit for service life. Degradation of alkaline water electrolyzer is mainly expected from hydride formation and hydrogen embrittlement of nickel components that are employed at the cathode.

In summary, on the basis of a rigorous scientific analysis, insights into the physicochemical processes of water splitting as well as the design of electrolyzers and their components are presented. The derived opportunities and challenges of acidic and alkaline low-temperature reactors should guide the way for the development and improvement of water electrolyzers to become an established key technology towards renewable energy conversion and storage.

ACKNOWLEDGEMENT

This research was supported by the German Federal Ministry of Education and Science (BMBF) under Grant No. 03EK3556.

References

1. J. H. Russell, L. J. Nuttall, and A. P. Fickett, *Am. Chem. Soc. Div. Fuel Chem., Prepr.* 18 (1973) 24.
2. M. Carmo, D. L. Fritz, J. Mergel, and D. Stolten, *Int. J. Hydrogen Energy*, 8 (2013) 4901.
3. K. Zeng and D. Zhang, *Prog. Energy Combust. Sci.*, 36 (2010) 307.
4. P. Vermeiren, W. Adriansens, J. Moreels, and R. Leysen, *Int. J. Hydrogen Energy* 23, (1998) 321.
5. H. Wendt and H. Hofmann, *J. Appl. Electrochem.*, 19 (1989) 605.
6. T. Metall and D. E. Hall, *J. Electrochem. Soc.*, (1981) 740.
7. D. L. Stojic, M. P. Marceta, S. P. Sovilj, and S. S. Miljanic, *J. Power Sources*, 118 (2003) 315.
8. W. Kreuter and H. Hofmann, *Int. J. Hydrogen Energy*, 23 (1998) 661.
9. L. Barreto, A. Makihira, and K. Riahi, *Int. J. Hydrogen Energy*, 28 (2003) 267.
10. C. White, R. Steeper, and A. Lutz, *Int. J. Hydrogen Energy*, 31 (2006) 1292.
11. B. L. Carrette, K. A. Friedrich, and U. Stimming, *Fuel Cells*, 1 (2001) 5.
12. M. W. Ellis, M. R. V. O. N. Spakovsky, and D. J. Nelson, *Proc. IEEE*, 89 (2001) 1808.
13. W. Wei and G. Jinlong, *Front. Chem. Sci. Eng.*, 5 (2010) 2.
14. G. A. Mills and F. W. Steffgen, *Catal. Rev.*, 8 (1974) 159.
15. M. E. Dry, *Catal. Today*, 71 (2002) 227.
16. J. Gretz, W. Korf and R. Lyons, *Int. J. Hydrogen Energy*, 16 (1991) 691.
17. A. R. Costa, D. Wagner, and F. Patisson, *J. Clean. Prod.* 46 (2013) 27.
18. R. Schlögel, in *Handb. Heterog. Catal.*, edited by G. Ertl, H. Knözinger, F. Schüth, and J. Weitkamp, *Wiley-VCH, Weinheim* (2008) 2501.
19. C. H. Hamann, A. Hamnett, and W. Vielstich in *Electrochemistry*, 2nd ed., *Wiley-VCH* (2007).
20. R. F. Mann, J. C. Amphlett, B. A. Peppley, and C. P. Thurgood, *J. Power Sources* 161, (2006) 775.
21. J. Divisek, P. Malinowski, J. Mergel, and H. Schmitz, *Int. J. Hydrogen Energy*, 10 (1985) 383.
22. A Brinner, H. Bussmann, W. Hug, and W. Seeger, *Int. J. Hydrogen Energy* 17, (1992) 187.
23. M. Schalenbach, W. Lueke, and D. Stolten, *J. Memb. Sci.*, 163 (2016) F1480.
24. F. Marangio, M. Santarelli, and M. Cali, *Int. J. Hydrogen Energy*, 34 (2009) 1143.
25. P. Haug, M. Koj, and T. Turek, *Int. J. Hydrogen Energy*, 49 (2017) 1.
26. P. Haug, B. Kreitz, M. Koj, and T. Turek, *Int. J. Hydrogen Energy*, 42 (2017) 15689.
27. M. Schalenbach, G. Tjarks, M. Carmo, W. Lueke, M. Mueller, and D. Stolten, *J. Electrochem. Soc.*, 163 (2016) F3197.

28. H. Ito, T. Maeda, A. Nakano, and H. Takenaka, *Int. J. Hydrogen Energy*, 36 (2011) 10527.
29. M. Schalenbach, M. Carmo, D. L. Fritz, J. Mergel, and D. Stolten, *Int. J. Hydrogen Energy*, 38 (2013) 14921.
30. M. Schalenbach, T. Hoefner, P. Paciok, M. Carmo, W. Lueke, and D. Stolten, *Phys. Chem. C*, 119 (2015) 25145.
31. P. H. Vermeiren, J. P. Moreels, and R. Leysen, *J. Porous Mater.*, 3 (1996) 33.
32. J. Divisek and P. Malinowski, *J. Electrochem. Soc.*, 133 (1982) 915.
33. J. Divisek, *J. Appl. Electrochem.*, 14 (1984) 663.
34. R. Renaud and R. Leroy, *Int. J. Hydrogen Energy* 7 (1982) 155.
35. L. J. Bonderer, P. W. Chen, P. Kocher, and L. J. Gauckler, *J. Am. Ceram. Soc.*, 93 (2010) 3624.
36. J. Etienne, A. Larbot, A. Julbe, C. Guizard, and L. Cot, *J. Memb. Sci.*, 86 (1994) 95.
37. M. Boaro and J. M. Vohs, *J. Am. Ceram. Soc.*, 86 (2003) 395.
38. J. C. Wu and L. Cheng, *J. Memb. Sci.*, 167 (2000) 253.
39. T. Yasuda, T. Okuno, and H. Yasuda, *Langemuir*, 10 (1994) 2435.
40. A. Nabe, E. Staude, and G. Belfort, *J. Memb. Sci.*, 133 (1997) 57.
41. I. Gancarz, G. Poz, and M. Bryjak, *Eur. Polym. J.*, 35 (1999) 1419.
42. P. Zoller and N. Buchs, *J. Polym. Sci.*, 16 (1978) 1261.
43. P. Zoller, *J. Polym. Sci.*, 20 (1982) 1453.
44. P. Vermeiren, W. Adriansens, and R. Leysen, *Int. J. Hydrog. Energy*, 21 (1996) 679.
45. Zirfon Perl UTP 500 data sheet, AGFA (2016).
46. T. A. Zawodzinski, C. Derouin, S. Radzinski, R. J. Sherman, V. T. Smith, T. E. Springer, and S. Gottesfeld, *J. Electrochem. Soc.*, 140 (1993) 1041.
47. T. A. Zawodzinski, T. E. Springer, J. Davey, R. Jestel, C. Lopez, J. Valeria, and S. Gottesfeld, *J. Electrochem. Soc.*, 140 (1993) 5.
48. R. W. Kopitzke, C. A. Linkous, H. R. Anderson, and G. L. Nelson, *J. Electrochem. Soc.*, 147 (2000) 1677.
49. E. Roche, M. Pineri, and R. Duplessix, *J. Polym. Sci.*, 20 (1982) 107.
50. K. D. Kreuer and G. Portale, *Mater. Views*, 23 (2013) 5390.
51. Nafion PFSA Membranes Data Sheet, DuPont Fuel Cells (http://www2.dupont.com/FuelCells/en_US/products/nafion.html, (2015)).
52. E. J. Roche, M. Pineri, R. Duplessix, and A. M. Levelut, *J. Polym. Sci. Polym. Phys. Ed.*, 19 (1981) 1.
53. F. I. Allen, L. R. Comolli, A. Kusoglu, M. A. Modestino, A. M. Minor, and A. Z. Weber, *ACS Macro Lett.*, 4 (2015) 1.
54. B. Smitha, S. Sridhar, and A. A. Khan, *J. Memb. Sci.*, 259 (2005) 10.
55. S. J. Peighambardoust, S. Rowshanzamir, and M. Amjadi, *Int. J. Hydrogen Energy*, 35 (2010) 9349.
56. S. Stucki, G. G. Scherer, S. Schlagowski, and E. Fischer, *J. Appl. Electrochem.*, 28 (1998) 1041.
57. M. Chandesris, V. Médeau, N. Guillet, S. Chelghoum, D. Thoby, and F. Fouda-Onana, *Int. J. Hydrogen Energy*, 40 (2015) 1353.
58. J. Healy, C. Hayden, T. Xie, K. Olson, R. Waldo, M. Brundage, H. Gasteiger, and J. Abbott, *Fuel Cells* 5 (2005) 302.
59. A. Collier, H. Wang, X. Ziyuan, J. Zhang, and D. Wilkinson, *Int J Hydrog. Energy*, 31 (2006) 1838.
60. C. S. Gittleman, F. D. Coms, and Y.-H. Lai, in *Polymer Electrolyte Fuel Cell Degradation*, Elsevier Inc., (2012), 15–88.
61. M. Inaba, T. Kinumoto, M. Kiriake, R. Umebayashi, A. Tasaka, and Z. Ogumi, *Electrochim Acta*, 51 (2006) 5746.
62. J. R. Varcoe and R. C. T. Slade, *Fuel Cells*, 5 (2005) 187.
63. G. Merle, M. Wessling, and K. Nijmeijer, *J. Memb. Sci.*, 377 (2011) 1.

64. O. I. Deavin, S. Murphy, A. L. Ong, S. D. Poynton, R. Zeng, H. Herman, and J. R. Varcoe, *Energy Environ. Sci.*, 5 (2012) 8584.
65. H. L. Yeager and A. Steck, *Anal. Chem.*, 51 (1979) 862.
66. H. Yeager and A. Steck, *J. Electrochem. Soc.*, 128 (1982) 1880.
67. A. Steck and H. Yeager, *Anal. Chem.*, 52 (1980) 1215.
68. D. Pletcher and X. Li, *Int. J. Hydrogen Energy*, 36 (2011) 15089.
69. R. S. Yeo, J. McBreen, G. Kissel, F. Kulesa, and S. Srinivasan, *J. Appl. Electrochem.* 10 (1980) 741.
70. M. Schalenbach, W. Lueke, W. Lehnert, and D. Stolten, *Electrochim. Acta*, 214 (2016) 362.
71. P. M. Sipos, G. Hefter, and P. M. May, *J. Chem. Eng. Data*, 45 (2000) 613.
72. I. Zaytsev and G. Aseyev in *Properties of Aqueous Solutions of Electrolytes*, CRC Press, Boca Raton, (1992).
73. National Institute of Standards and Technology, <http://webbook.nist.gov/chemistry/fluid/>.
74. N. Uddin, J. Kim, B. J. Sung, T. H. Choi, C. H. Choi, and H. Kang, *J. Phys. Chem.*, B 118 (2014) 13671.
75. D. Marx, *Chemphyschem*, 7 (2006) 1848.
76. N. Agmon, *Chem. Phys. Lett.*, 244 (1995) 456.
77. A. B. Duso and D. D. Y. Chen, *Anal. Chem.*, 74 (2002) 2938.
78. T. A. Zawodzinski, J. Davey, J. Valerio, and S. Gottesfeld, *Electrochim. Acta* 40, 297 (1995).
79. K. Onda, T. Murakami, T. Hikosaka, M. Kobayashi, R. Notu, and K. Ito, *J. Electrochem. Soc.*, 149 (2002) A1069.
80. R. Gilliam, J. Graydon, D. Kirk, and S. Thorpe, *Int. J. Hydrogen Energy*, 32 (2007) 359.
81. W. J. Hamer and H. J. DeWane, *Natl. Stand. Ref. Data Syst.*, 33 (1970) 1.
82. T. A. Zawodzinski, C. Derouin, S. Radzinski, R. J. Sherman, V. T. Smith, T. E. Springer, and S. Gottesfeld, *J. Electrochem. Soc.*, 140 (1993) 1041.
83. K.-D. Kreuer, *Solid State Ionics*, 252 (2013) 93.
84. C. E. Evans, R. D. Noble, S. Nazeri-Thompson, B. Nazeri, and C. A. Koval, *J. Memb. Sci.*, 279 (2006) 521.
85. F. Lufrano, G. Squadrito, A. Patti, and E. Passalacqua, *J. Appl. Polym. Sci.*, 77 (2000) 1250.
86. P. Ruetschi and R. F. Amlie, *J. Phys. Chem.*, 70 (1966) 718.
87. K. E. Gubbins and R. D. J. Walker, *J. Electrochem. Soc.*, 112 (1965) 469.
88. M. K. Tham, R. D. Walker, and K. E. Gubbins, *J. Phys. Chem.*, 74 (1970) 1747.
89. M. Schalenbach, M. Hoeh, J. Gostick, W. Lueke, and D. Stolten, *Phys. Chem. C*, 119 (2015) 25156.
90. K. Kikuchi, Y. Tanaka, Y. Saihara, and Z. Ogumi, *Electrochim. Acta*, 52 (2006) 904.
91. K. Kikuchi, S. Nagata, Y. Tanaka, Y. Saihara, and Z. Ogumi, *J. Electroanal. Chem.*, 600 (2007) 303.
92. Y. Tanaka, K. Kikuchi, Y. Saihara, and Z. Ogumi, *Electrochim. Acta*, 50 (2005) 5229.
93. K. Kikuchi, Y. Tanaka, Y. Saihara, M. Maeda, M. Kawamura, and Z. Ogumi, *J. Colloid Interface Sci.*, 298 (2006) 914.
94. Y. Tanaka, S. Uchinashi, Y. Saihara, K. Kikuchi, T. Okaya, and Z. Ogumi, *Electrochim. Acta*, 48 (2003) 4013.
95. S. J. Osborn, M. K. Hassan, G. M. Divoux, D. W. Rhoades, K. A. Mauritz, and R. B. Moore, *Macromolecules*, 40 (2007) 3886.
96. F. Bauer, S. Dennerler, and M. Willert-Porada, *J. Polym. Sci. Part B Polym. Phys.*, 43 (2005) 786.
97. S. Kundu, L. C. Simon, M. Fowler, and S. Grot, *Polymer*, 46 (2005) 11707.
98. A. Kusoglu, A. M. Karlsson, M. H. Santare, S. Cleghorn, and W. B. Johnson, *J. Power Sources*, 170 (2007) 345.
99. Y. Tang, A. M. Karlsson, M. H. Santare, M. Gilbert, S. Cleghorn, and W. B. Johnson, *Mater. Sci. Eng. A*, 425 (2006) 297.

100. T. L. Barr, *J. Phys. Chem.*, 82 (1978) 1801.
101. M. Peuckert, F. Coenen, and H. Bonzel, *Electrochim. Acta*, 29 (1984) 1305.
102. B. S. Yeo and A. T. Bell, *Phys. Chem. C*, 116 (2012) 8394.
103. D. S. Hall, D. J. Lockwood, S. Poirier, C. Bock, and B. R. MacDougall, *ACS Appl. Mater. Inter.*, 6 (2014) 3141.
104. D. Davies and W. Barker, *Corros. - Natl. Assoc. Corros. Eng.*, 20 (1964) 47t.
105. M. Alsabet, M. Grden, and G. Jerkiewicz, *Electrocatal.*, 2 (2011) 317.
106. M. Alsabet, M. Grden, and G. Jerkiewicz, *Electrocatal.*, 5 (2014) 136.
107. S. Geiger, S. Cherevko, and K. J. J. Mayrhofer, *Electrochim. Acta*, 179 (2015) 24.
108. S. Ahn, H. Kwon, and D. D. Macdonald, *Electrochim. Acta*, 152 (2005) B482.
109. U. Stimming and J. W. Schultze, *Berichte Der Bunsengesellschaft Für Phys. Chemie*, 80 (1976) 1297.
110. J. O. Bockris, A. K. N. Reddy, and B. Rao, *J. Electrochem. Soc.*, 113 (1966) 1133.
111. T. Dickinson, A. F. Povey, and P. M. A. Sherwood, *J. Chem.*, 73 (1977) 327.
112. A. Kowal, R. Niewiara, B. Peroczyk, and J. Haber, *Langmuir*, 12 (1996) 2332.
113. S. F. Lincoln, D. T. Richens, and A. G. Sykes, in *Compr. Coord. Chem. II* (2004) 515.
114. Pourbaix M. in *Atlas of Electrochemical Equilibria in Aqueous Solutions, NACE International*, 2nd ed. (1974).
115. N. D. Lang and W. Kohn, *Phys. Rev. B*, 3 (1971) 1215.
116. H. B. Michaelson, *J. Appl. Phys.*, 48 (1977) 4729.
117. P. Vanýsek in *Handb. Chem. Phys., Taylor and Francis Group*, 95th ed. (2014) 5_80.
118. B. Hammer and J. K. Nørskov, *Nature*, 376 (1995) 238.
119. J. O. M. Bockris and S. D. Argade, *J. Chem. Phys.*, 49 (1968) 5133.
120. W. Haynes in *CRC Handb. Chem. Phys., Taylor and Francis Group*, 96th ed. (2016), 14.
121. S. Cherevko, A. R. Zeradjanin, A. A. Topalov, N. Kulyk, I. Katsounaros, and K. J. J. Mayrhofer, *ChemCatChem*, 6 (2014) 2219.
122. M. Schalenbach, O. Kasian, M. Ledendecker, S. Cherevko, A. Mingers, F. Speck, and K. J. J. Mayrhofer, *Electrocatalysis*, DOI: 10.1007/s12678-017-0438-y, (2017).
123. L. M. Roen, C. H. Paik, and T. D. Jarvi, *Electrochem. Solid-State Lett.*, 7 (2004) A19.
124. A. A. Topalov, S. Cherevko, A. R. Zeradjanin, J. C. Meier, I. Katsounaros, and K. J. J. Mayrhofer, *Chem. Sci.*, 5 (2014) 631.
125. S. Cherevko, S. Geiger, O. Kasian, N. Kulyk, J. P. Grote, A. Savan, B. R. Shrestha, S. Merzlikin, B. Breitbach, A. Ludwig, and K. J. J. Mayrhofer, *Catal. Today*, 262 (2016) 170.
126. R. Kötz, H. Neff, and S. Stucki, *J. Electrochem. Soc.*, 131 (1984) 72.
127. A. Minguzzi, O. Lugaresi, E. Achilli, C. Locatelli, A. Vertova, P. Ghignabac, and S. Rondininiac, *Chem. Sci.* 5 (2014) 3591.
128. H. G. Sanchez Casalongue, M. L. Ng, S. Kaya, D. Friebel, H. Ogasawara, and A. Nilsson, *Angew. Chemie*, 126 (2014) 7297.
129. V. Pfeifer, T. E. Jones, J. J. V. Velez, C. Massue, M. T. Greiner, R. Arrigo, D. Teschner, F. Girgsdies, M. Scherzer, J. Allan, M. Hashagen, G. Weinberg, S. Piccinin, M. Hävecker, A. Knop-Gericke, and R. Schloegel, *PCCP*, 18 (2016) 2292.
130. M. E. G. Lyons, R. L. Doyle, I. Godwin, M. O. Brien, and L. Russell, 159 (2012) 932.
131. O. Diaz-Morales, D. Ferrus-Suspedra, and M. T. M. Koper, *Chem. Sci.*, 7 (2016) 2639.
132. T. Binninger, R. Mohamed, K. Waltar, E. Fabbri, P. Levecque, R. Kötz, and T. J. Schmidt, *Scien. Rep.*, (2015) 1.
133. V. Pfeifer, T. E. Jones, J. V. Vélez, C. Massué, R. Arrigo, D. Teschner, F. Girgsdies, M. Scherzer, M. T. Greiner, J. Allan, M. Hashagen, G. Weinberg, S. Piccinin, M. Hävecker, A. Knop-Gericke, and R. Schlögl, *Surf. Interface Anal.* 48 (2015) 261.
134. A. R. Despic and V. D. Jovic, in *Modern Aspects of Electrochemistry, Springer Science+Buisness Media*, (1995) 143.

135. D. E. Williams, *Nature*, 350 (1991) 216.
136. A. Machet, A. Galtayries, S. Zanna, L. Klein, V. Maurice, P. Jolivet, M. Foucault, P. Combrade, P. Scott, and P. Marcus, *Electrochim. Acta*, 49 (2004) 3957.
137. I. Olefjord, *J. Electrochem. Soc.*, 132 (1985) 2854.
138. A. E. Yaniv, *J. Electrochem. Soc.*, 124 (1977) 490.
139. L. Olefjord and C. R. Clayton, *ISIJ Int.*, 31 (1991) 134.
140. K. J. J. Mayrhofer, V. Juhart, K. Hartl, M. Hanzlik, and M. Arenz, *Angew. Chemie - Int. Ed.*, 48 (2009) 3529.
141. D. M. Soares, *J. Electrochem. Soc.*, 139 (1992) 98.
142. D. S. Hall, C. Bock, and B. R. Macdougall, *J. Electrochem. Soc.*, 160 (2013) F235.
143. S. Lynch, *Scr. Metall.*, 12 (1979) 1051.
144. M. Louthan, G. Caskey, J. Donovan, and D. Rawl, *Mater. Sci. Eng.*, 10 (1972) 357.
145. R. Walter, R. Jewett, and W. Chandler, *Mater. Sci. Eng.*, 5 (1970) 98.
146. I. De France, D. Matriaux, and L. Renardires, *Int. J. Hydrogen Energy*, 18 (1993) 561.
147. J. A. Bett, K. Kinoshita, and P. Stonehart, *J. Catal.*, 35 (1974) 307.
148. P. Parthasarathy and A. V. Virkar, *J. Power Sources*, 234 (2013) 82.
149. J. C. Meier, C. Galeano, I. Katsounaros, A. A. Topalov, A. Kostka, F. Schüth, and K. J. J. Mayrhofer, *ACS Catal.*, 2 (2012) 832.
150. J. C. Meier, I. Katsounaros, C. Galeano, H. J. Bongard, A. A. Topalov, A. Kostka, A. Karschin, F. Schüth, and K. J. J. Mayrhofer, *Energy Environ. Sci.*, 5 (2012) 9319.
151. M. H. Miles and M. A. Thomason, *J. Electrochem. Soc.*, 123 (1979) 1459.
152. B. Hammer, *Adv. Catal.*, 45 (2000) 71.
153. B. Conway and J. O. M. Bockris, *Nature*, 178 (1956) 488.
154. R. Parsons, *Trans. Faraday Soc.*, 54 (1958) 1053.
155. W. Hong, M. Risch, K. A. Stoerzinger, A. J. L. Grimaud, J. Suntivich, and Y. Shao-Horn, *Energy Environ. Sci.*, 8 (2015) 1404.
156. M. T. M. Koper, *J. Electroanal. Chem.*, 660 (2011) 254.
157. N. M. Markovic, S. T. Sarraf, H. A. Gasteigert, and P. N. Ross, *J. Chem. Cos. Faraday Trans.*, 92 (1996) 3719.
158. N. M. Markovic, B. N. Grgur, and P. N. Ross, *J. Phys. Chem.*, B 101 (1997) 5405.
159. J. Durst, A. Siebel, C. Simon, F. Hasché, J. Herranz, and H. A. Gasteiger, *Energy Environ. Sci.*, 7 (2014) 2255.
160. K. C. Neyerlin, W. Gu, J. Jorne, and H. A. Gasteiger, *J. Electrochem. Soc.*, 154 (2007) B631.
161. W. Sheng, H. A. Gasteiger, and Y. Shao-Horn, *J. Electrochem. Soc.*, 157 (2010) B1529.
162. W. Sheng, Z. Zhuang, M. Gao, J. Zheng, J. G. Chen, and Y. Yan, *Nat. Commun.*, 6 (2015) 1.
163. J. Zheng, W. Sheng, Z. Zhuang, B. Xu, and Y. Yan, *Sci. Adv.*, 2 (2016) 1.
164. W. Sheng, M. Myint, J. G. Chen, and Y. Yan, *Energy Environ. Sci.*, 6 (2013) 1509.
165. L. Krishtalik, *Adv. Electrochem. Electrochem. Eng.*, 7 (1970) 283.
166. J. Nørskov, T. Bligaard, A. Logadottir, J. R. Kitchin, J. G. Chen, S. Pandelov, and U. Stimming, *J. Electrochem. Soc.*, 152 (2005) J23.
167. P. Quaino, F. Juárez, E. Santos, and W. Schmickler, *Beilstein J. Nanotechnol.*, 5 (2014) 846.
168. W. Schmickler and S. Trasatti, *J. Electrochem. Soc.*, 153 (2006) L31.
169. P. Rüetschi and P. Delahay, *J. Chem. Phys.*, 23 (1955) 195.
170. S. Trasatti, *Electroanal. Chem. Interfacial Electrochem.*, 39 (1972) 163.
171. E. Santos, P. Quaino, and W. Schmickler, *PCCP*, 14 (2012) 11224.
172. A. R. Zeradjanin, J. P. Grote, G. Polymeros, and K. J. J. Mayrhofer, *Electroanal.*, 28 (2016) 2256.
173. S. Trasatti, *J. Chem. Soc. Faraday Trans.*, 1 (1972) 229.
174. S. Trasatti, *J. Electroanal. Chem. Int. Electrochem.*, 123 (1981) 121.
175. J. Rossmeisl, A. Logadottir, and J. K. Nørskov, *Chem. Phys.*, 319 (2005) 178.

176. J. Rossmeisl, Z.-W. Qu, H. Zhu, G.-J. Kroes, and J. K. Nørskov, *J. Electroanal. Chem.*, 607 (2007) 83.
177. I. C. Man, H.-Y. Su, F. Calle-Vallejo, H. A. Hansen, J. I. Martínez, N. G. Inoglu, J. Kitchin, T. F. Jaramillo, J. K. Nørskov, and J. Rossmeisl, *ChemCatChem*, 3 (2011) 1159.
178. V. Viswanathan, H. A. Hansen, J. Rossmeisl, and J. K. Nørskov, *ACS Catal.*, 2 (2012) 1654.
179. I. Katsounaros, S. Cherevko, A. R. Zeradjanin, and K. J. J. Mayrhofer, *Angew. Chem. Int. Ed.*, 53 (2014) 102.
180. D. Chen, C. Chen, Z. M. Baiyee, Z. Shao, and F. Ciucci, *Chem. Rev.*, 115 (2015) 9869.
181. S. Trasatti, *Encycl. Electrochem. Power Sources*, 1 (2009) 49.
182. M. Zhang, M. De Respinis, and H. Frei, *Nat. Chem.*, 6 (2014) 362.
183. L. Giordano, B. Hanb, M. Risch, W. T. Hong, R. R. Rao, K. A. Stoerzinger, and Y. Shao-Horn, *Catal. Today*, 262 (2015) 2.
184. W. Ryden and A. Lawson, *Phys. Lett.*, 26A (1968) 209.
185. L. Trotochaud, S. L. Young, J. K. Ranney, and S. W. Boettcher, *J. Am. Chem. Soc.*, 136 (2014) 6744.
186. M. Nesselberger, S. Ashton, J. C. Meier, I. Katsounaros, K. J. J. Mayrhofer, and M. Arenz, *J. Am. Chem. Soc.*, 133 (2011) 17428.
187. T. Reier, M. Oezaslan, and P. Strasser, *ACS Catal.*, 2 (2012) 1765.
188. S. Trasatti and O. A. Petrii, *J. Electroanal. Chem.*, 327 (1992) 353.
189. J. R. Macdonald and C. A. J. Barlow, *J. Chem. Phys.*, 36 (1962) 3062.
190. T. Pajkossy, *J. Electroanal. Chem.*, 364 (1994) 111.
191. T. Pajkossy, *Solid State Ionics*, 176 (2005) 1997.
192. C. C. L. McCrory, S. Jung, J. C. Peters, and T. F. Jaramillo, *J. Am. Chem. Soc.*, 135 (2013) 16977.
193. C. C. L. McCrory, S. Jung, I. M. Ferrer, S. M. Chatman, J. C. Peters, and T. F. Jaramillo, *J. Am. Chem. Soc.*, 137 (2015) 4347.
194. B. E. Conway and L. Bai, *J. Electroanal. Chem.*, 198 (1986) 149.
195. U. Heiz, A. Sanchez, S. Abbet, and W. Schneider, *J. Am. Chem. Soc.*, 121 (1999) 3214.
196. M. Watt-Smith, J. Friedrich, S. Rigby, T. Ralph, and F. Walsh, *J. Phys. D Appl. Phys.*, 41 (2008) 1.
197. J. C. K. Ho and H. Thus, *J. Appl. Electrochem.*, 26 (1996) 515.
198. M. Shao, J. H. Odell, S. Choi, and Y. Xia, *Electrochem. Commun.*, 31 (2013) 46.
199. D. S. Hall, C. Bock, and B. R. MacDougall, *J. Electrochem. Soc.*, 161 (2014) H787.
200. E. Herrero, L. J. Buller, and H. D. Abruna, *Chem. Rev.*, 101 (2001) 1897.
201. R. F. Savinell, R. L. Zeller, and J. A. Adams, *J. Electrochem. Soc.*, 137 (1990) 489.
202. S. M. Alia, K. E. Hurst, S. S. Kocha, and B. S. Pivovar, *J. Electrochem. Soc.*, 163 (2016) F3051.
203. S. Ardizzone, G. Fregonara, and S. Trasatti, *Electrochim. Acta*, 35 (1989) 263.
204. M. Schalenbach, M. Ledendecker, O. Kasian, S. Cherevko, and K. Mayrhofer, *in work*, (2017).
205. M. Schalenbach, F. D. Speck, M. Ledendecker, O. Kasian, D. Goehl, A. M. Mingers, B. Breitbach, H. Springer, S. Cherevko, and K. J. J. Mayrhofer, *Electrochim. Acta*, DOI:10.1016/j.electacta.2017.11.069, (2017).
206. J. M. Doña Rodríguez, J. A. Herrera Melián, and J. Pérez Peña, *J. Chem. Educ.*, 77 (2000) 1195.
207. S. Brunauer, P. H. Emmett, and E. Teller, *J. Am. Chem. Soc.*, 60 (1938) 309.
208. K. S. W. Sing, *Adv. Colloid Interface Sci.*, 76-77 (1998) 3.
209. Q. Lu, G. S. Hutchings, W. Yu, Y. Zhou, R. V Forest, R. Tao, J. Rosen, B. T. Yonemoto, Z. Cao, H. Zheng, J. Q. Xiao, F. Jiao, and J. G. Chen, *Nat. Commun.*, 6 (2015) 1.
210. J. Erlebacher, M. Aziz, A. Karma, N. Dimitrov, and K. Sieradzki, *Nature* 410 (2001) 450.
211. J. Erlebacher, *J. Electrochem. Soc.*, 151 (2004) C614.
212. J. Erlebacher and K. Sieradzki, *Scr. Mater.*, 49 (2003) 991.
213. N. Menzel, E. Ortel, R. Kraehnert, and P. Strasser, *ChemPhysChem.*, 13 (2012) 1385.

214. J. Luo, L. Wang, D. Mott, P. N. Njoki, Y. Lin, T. He, Z. Xu, B. N. Wanjana, I. I. S. Lim, and C. J. Zhong, *Adv. Mater.*, 20 (2008) 4342.
215. X. Lai, J. E. Halpert, and D. Wang, *Energy Environ. Sci.*, 5 (2012) 5604.
216. Y. Song, Y. Yang, C. J. Medforth, E. Pereira, A. K. Singh, H. Xu, Y. Jiang, C. J. Brinker, F. Van Swol, and J. A. Shelnett, *J. Am. Chem. Soc.*, 126 (2004) 635.
217. S. Sun, F. Jaouen, and J. P. Dodelet, *Adv. Mater.*, 20 (2008) 3900.
218. C. Chen, Y. Kang, Z. Huo, Z. Zhu, W. Huang, H. L. Xin, J. D. Snyder, D. Li, J. A. Herron, M. Mavrikakis, M. Chi, K. L. More, Y. Li, N. M. Markovic, G. Somorjai, P. Yang, and V. R. Stamenkovic, *Science*, 343 (2014) 1339.
219. L. Zhang, L. T. Roling, X. Wang, M. Vara, M. Chi, J. Liu, S.-I. Choi, J. Park, J. A. Herron, Z. Xie, M. Mavrikakis, and Y. Xia, *Science*, 349 (2015) 412.
220. H. Shen, W. Xu, and P. Chen, *PCCP*, 12 (2010) 6555.
221. G. S. Attard, P. N. Bartlett, N. R. B. Coleman, J. M. Elliott, J. R. Owen, and J. H. Wang, *Science*, 278 (1997) 838.
222. V. Ganesh and V. Lakshminarayanan, *Electrochim. Acta*, 49 (2004) 3561.
223. C. Baldizzone, L. Gan, N. Hodnik, G. P. Keeley, A. Kostka, M. Heggen, P. Strasser, and K. J. J. Mayrhofer, *ACS Catal.*, 5 (2015) 5000.
224. J. Greeley, T. F. Jaramillo, J. Bonde, I. B. Chorkendorff, and J. K. Nørskov, *Nat. Mater.*, 5 (2006) 909.
225. R. Gomer, *Rep. Prog. Phys.*, 53 (1990) 917.
226. G. X. Cao, E. Nabighian, and X. D. Zhu, *Phys. Rev. Lett.*, 79 (1997) 3696.
227. X. D. Zhu, A. Lee, and A. Wongal, *Phys. Rev. Lett.*, 68 (1992) 1862.
228. A. Von Oertzen, H. H. Rotermund, and S. Nettesheim, *Surf. Sci.*, 311 (1994) 322.
229. M. R. Gennero de Chialvo, A. C. Chialvo, *J. Electroanal. Chem.*, 448 (1998) 87.
230. C. Fan, D. L. Piron, A. Slebo, and P. Paradis, *J. Electrochem. Soc.*, 141 (1994) 382.
231. J. M. Jaksic, M. V. Vojnovic, and N. V. Krstajic, *Electrochim. Acta*, 45 (2000) 4151.
232. M. Metikos-Hukovic and A. Jukic, *Electrochim. Acta*, 45 (2000) 4159.
233. M. M. Jaksic, *Int. J. Hydrogen Energy*, 26 (2001) 559.
234. S. G. Neophytides, S. Zafeiratos, G. D. Papakonstantinou, J. M. Jaksic, F. E. Paloukis, and M. M. Jaksic, *Int. J. Hydrogen Energy*, 30 (2005) 131.
235. S. G. Neophytides, S. Zafeiratos, G. D. Papakonstantinou, J. M. Jaksic, F. E. Paloukis, and M. M. Jaksic, *Int. J. Hydrogen Energy*, 30 (2005) 393.
236. J. G. Highfield, E. Claude, and K. Oguro, *Electrochim. Acta*, 44 (1999) 2805.
237. M. Ledendecker, J. Mondschein, O. Kasian, S. Geiger, D. Göhl, M. Schalenbach, A. Zeradjanin, S. Cherevko, R. E. Schaak, and K. Mayrhofer, *Angew. Chemie Int. Ed.*, (2017).
238. E. Fabbri, A. Habereder, K. Waltar, R. Kötz, and T. J. Schmidt, *Catal. Sci. Technol.*, 4 (2014) 3800.
239. M. Risch, A. Grimaud, K. J. May, K. A. Stoerzinger, T. J. Chen, A. N. Mansour, and Y. Shao-horn, *J. Phys. Chem.*, 117 (2013) 8628.
240. Y. Lee, A. Grimaud, and Y. Shao-horn, *J. Phys. Chem. Lett.*, 3 (2012) 3264.
241. D. A. Corrigan, *J. Electrochem. Soc.*, 134 (1980) 377.
242. D. A. Corrigan and R. M. Bendert, *J. Electrochem. Soc.*, 136 (1989) 723.
243. L. J. Enman, M. S. Burke, A. S. Batchellor, and S. W. Boettcher, *ACS Catal.*, 6 (2016) 2416.
244. D. Friebel, M. W. Louie, M. Bajdich, K. E. Sanwald, Y. Cai, A. M. Wise, M. Cheng, D. Sokaras, T. Weng, R. Alonso-mori, R. C. Davis, J. R. Bargar, J. K. Nørskov, A. Nilsson, and A. T. Bell, *J. Am. Chem. Soc.*, 137 (2015) 1305.
245. Y. Li and A. Selloni, *ACS Catal.*, 4 (2014) 1148.
246. K. Gong, F. Du, Z. Xia, M. Durstock, and L. Dai, *Science*, 323 (2009) 760.
247. S. Chen, J. Duan, M. Jaroniec, and S. Z. Qiao, *Adv. Mater.*, 26 (2014) 2925.
248. X. Lu, W. L. Yim, B. H. R. Suryanto, and C. Zhao, *J. Am. Chem. Soc.*, 137 (2015) 2901.

249. H. T. Chung, J. H. Won, and P. Zelenay, *Nat. Commun.*, 4 (2013) 1922.
250. D. R. P. Morris, S. P. Liu, D. V. Gonzalez, and J. T. Gostick, *ACS Appl. Mater. Interfaces*, 6 (2014) 18609.
251. R. Makharia, M. F. Mathias, and D. R. Baker, *J. Electrochem. Soc.*, 152 (2005) A970.
252. C. Boyer, S. Gamburgzev, O. Velev, S. Srinivasan, and A. J. Appleby, *Electrochim Acta*, 43 (1998) 3703.
253. R. O'Hayre, D. M. Barnett, and F. B. Prinz, *J. Electrochem. Soc.*, 152 (2005) A439.
254. C. Gabrielli, F. Huet, M. Keddad, A. Macias, and A. Sahar, *J. Appl. Electrochem.*, 19 (1989) 617.
255. J. Eigeldinger and H. Vogt, *Electrochim. Acta*, 45 (2000) 4449.
256. J. Dukovic and C. W. Tobias, *J. Electrochem. Soc.*, 134 (1986) 331.
257. W. Xu and K. Scott, *Int. J. Hydrogen Energy*, 35 (2010) 12029.
258. S. Siracusano, V. Baglio, A. Stassi, L. Merlo, E. Moukheiber, and A. S. Arico, *J. Memb. Sci.*, 466 (2014) 1.
259. E. Antolini, *Appl. Catal. B Environ.*, 88 (2009) 1.
260. M. Uchida, Y. Fukuoka, Y. Sugawara, N. Eda, and A. Ohta, *J. Electrochem. Soc.*, 143 (1996) 2245.
261. A. E. Aksoylu, M. Madalena, A. Freitas, M. F. R. Pereira, and J. L. Figueiredo, *Carbon*, 39 (2001) 175.
262. J. Xu, G. Liu, J. Li, and X. Wang, *Electrochim. Acta*, 59 (2012) 105.
263. Y. Kamegaya, K. Sasaki, M. Oguri, T. Asaki, H. Kobayashi, and T. Mitamura, *Electrochim. Acta*, 40 (1995) 889.
264. S. M. A. Shibli and V. S. Dilimon, *Int. J. Hydrogen Energy*, 33 (2008) 1104.
265. A. Kusoglu, A. Kwong, K. T. Clark, H. P. Gunterman, and A. Z. Weber, *J. Electrochem. Soc.*, 159 (2012) F530.
266. C. Ziegler, S. Thiele, and R. Zengerle, *J. Power Sources*, 196 (2011) 2094.
267. W. K. Epting, J. Gelb, and S. Litster, *Mater. Views*, 22 (2012) 555.
268. V. Mehta and J. S. Cooper, *J. Power Sources*, 114 (2003) 32.
269. N. Rajalakshmi and K. S. Dhathathreyan, *Chem. Eng. J.*, 129 (2007) 31.
270. M. S. Wilson, and S. Gottesfeld, *J. Appl. Electrochem.*, 22 (1992) 1.
271. H. Su, B. J. Bladergroen, V. Linkov, S. Pasupathi, and S. Ji, *Int. J. Hydrogen Energy*, 36 (2011) 15081.
272. A. D. Taylor, E. Y. Kim, V. P. Humes, J. Kizuka, and L. T. Thompson, *J. Power Sources*, 171 (2007) 101.
273. J. H. Cho, J. M. Kim, J. Prabhuram, S. Y. Hwang, D. J. Ahn, H. Y. Ha, and S. K. Kim, *J. Power Sources*, 187 (2009) 378.
274. M. S. Saha, D. K. Paul, B. A. Peppley, and K. Karan, *Electrochem. Commun.*, 12 (2010) 410.
275. G. Schiller, R. Henne, P. Mohr, and V. Peinecke, *Int. J. Hydrogen Energy*, 23 (1998) 761.
276. G. Schiller, R. Henne, and V. Borck, *J. Therm. Spray Technol.*, 4 (1995) 185.
277. Y. Tan, H. Wang, P. Liu, Y. Shen, C. Cheng, A. Hirata, T. Fujita, Z. Tang, and M. Chen, *Energy Environ. Sci.*, 9 (2016) 2257.
278. J. S. Chen, J. Ren, M. Shalom, T. Fellingner, and M. Antonietti, *ACS Appl. Mater. Interfaces*, 8 (2016) 5509.
279. J. Y. Huot, M. L. Trudeau, and R. Schulz, *J. Electrochem. Soc.*, 138 (1991) 1316.
280. H. Lubanska, *J. Met.*, 22 (1970) 45.
281. A. Inoue, K. Kita, K. Ohtera, H. Kimura, and T. Masumoto, *J. Mater. Sci. Lett.*, 7 (1988) 1287.
282. G. Davies and S. Zhen, *J. Mater. Sci.*, 18 (1983) 1899.
283. B. V. Paserin, S. Marcuson, J. Shu, and D. S. Wilkinson, *Adv. Eng. Mater.*, 6 (2004) 454.
284. W. Liu and N. Canfield, *J. Memb. Sci.*, 409-410 (2012) 113.
285. D. Miousse, A. Lasia, and V. Borck, *J. Appl. Electrochem.*, 25 (1995) 592.
286. M. Metikos-Hukovic, Z. Grubac, N. Radic, and A. Tonejc, *J. Mol. Catal.*, 249 (2006) 172.

287. S. Cherevko, and C.H. Chung, *Electrochem. Comm.*, 13 (2011) 16.
288. C. A. Marozzi and A. C. Chialvo, *Electrochim. Acta*, 45 (2000) 2111.
289. N. V. Krstajić, V. D. Jović, L. Gajić-Krstajić, B. M. Jović, A. L. Antozzi, and G. N. Martelli, *Int. J. Hydrogen Energy*, 33 (2008) 3676.
290. Q. Han, S. Cui, N. Pu, J. Chen, K. Liu, and X. Wei, *Int. J. Hydrogen Energy*, 35 (2010) 5194.
291. L. Xu, Y. Ding, C. Chen, L. Zhao, C. Rimkus, R. Joesten, and S. L. Suib, *Chem. Mater.*, 20 (2008) 308.
292. M. Zeng, H. Wang, C. Zhao, J. Wei, K. Qi, and W. Wang, *ChemCatChem*, 8 (2016) 708.
293. Y. Chai, X. Shang, G. Han, B. Dong, W. Hu, and Y. Liu, *Int. J. Electrochem. Sci.*, 11 (2016) 3050.
294. R. J. C. Brown, P. J. Brewer, and M. J. T. Milton, *J. Mat. Chem.*, 230 (2002) 2749.
295. Q. Liu, S. Gu, and C. M. Li, *J. Power Sources*, 299 (2015) 342.
296. P. Zhang, M. Wang, Y. Yang, T. Yao, H. Han, and L. Sun, *Nano Energy*, 19 (2016) 98.
297. C. C. Hu, C. H. Tsay, and A. Bai, *Electrochim. Acta*, 48 (2003) 907.
298. E. Chassaing, K. V. Quang, and R. Wiart, *J. Appl. Electrochem.*, 17 (1987) 1267.
299. A. P. Abbott and K. J. McKenzie, *PCCP*, 8 (2006) 4265.
300. L. Ghassemzadeh, K. D. Kreuer, J. Maier, and K. Müller, *J. Power Sources*, 196 (2011) 2490.
301. M. J. Kelly, G. Fafilek, J. O. Besenhard, H. Kronberger, and G. E. Nauer, *J. Power Sources*, 145 (2005) 249.
302. N. E. Cipollini, *ECS Trans.*, 11 (2007) 1071.
303. M. D. Earle, *Phys. Rev.*, 614 (1942) 56.
304. S. A. Grigoriev, P. Millet, S. A. Volobuev, and V. N. Fateev, *Int. J. Hydrogen Energy*, 34 (2009) 4968.
305. A. S. Gago, S. A. Ansar, B. Saruhan, U. Schulz, P. Lettenmeier, N. A. Cañas, P. Gazdzicki, T. Morawietz, R. Hiesgen, J. Arnold, and K. A. Friedrich, *J. Power Sources*, 307 (2016) 815.
306. I. Nitta, O. Himanen, and M. Mikkola, *Electrochem. Commun.*, 10 (2008) 47.
307. J. Ge, A. Higier, and H. Liu, *J. Power Sources*, 159 (2006) 922.
308. W. K. Lee, C. H. Ho, J. W. Van Zee, and M. Murthy, *J. Power Sources*, 84 (1999) 45.
309. R. L. LeRoy, C. T. Bowen, and D. J. LeRoy, *J. Electrochem. Soc.*, 127 (1980) 1954.
310. P. H. Huang, *ECS Trans.*, 12 (2008) 479.
311. J. Balej, *Int. J. Hydrogen Energy*, 10 (1985) 233.
312. H. Janssen, J. Bringmann, B. Emonts, and V. Schroeder, *Int. J. Hydrogen Energy*, 29 (2004) 759.
313. S. A. Grigoriev, P. Millet, S. V. Korobtsev, V. I. Porembskiy, M. Pepic, C. Etievant, C. Puyenchet, and V. N. Fateev, *Int. J. Hydrogen Energy*, 34 (2009) 5986.
314. J. Divisek, R. Jung, and D. Britz, *J. Appl. Electrochem.*, 20 (1990) 186.
315. S. Sun, Z. Shao, H. Yu, G. Li, and B. Yi, *J. Power Sources*, 267 (2014) 515.
316. M. K. Kadirov, A. Bosnjakovic, and S. Schlick, *J. Phys. Chem. B*, 109 (2005) 7664.
317. M. Danilczuk, F. D. Coms, and S. Schlick, *Fuel Cells*, 8 (2008) 436.
318. M. Danilczuk, F. D. Coms, and S. Schlick, *J. Phys. Chem. B*, 113 (2009) 8031.
319. B. Vogel, E. Aleksandrova, S. Mitov, M. Krafft, A. Dreizler, J. Kerres, M. Hein, and E. Roduner, *J. Electrochem. Soc.*, 155 (2008) B570.
320. Y. Nosaka, K. Ohtaka, N. Ohguri, and A. Y. Nosaka, *J. Electrochem Soc.*, 158 (2011) B430.
321. L. Ghassemzadeh and S. Holdcroft, *J. Am. Chem. Soc.*, 135 (2013) 8181.
322. S. A. Grigoriev, K. A. Dzhus, D. G. Bessarabov, and P. Millet, *Int. J. Hydrogen Energy*, 39 (2014) 20440.
323. C. Rozain, E. Mayousse, N. Guillet, and P. Millet, *Appl. Catal. B Environ.*, 182 (2016) 123.
324. S. Cherevko, T. Reier, A. R. Zeradhanin, Z. Pawolek, P. Strasser, and K. J. J. Mayrhofer, *Electrochem. Commun.*, 48 (2014) 81.
325. C. Rakousky, U. Reimer, K. Wippermann, M. Carmo, W. Lueke, and D. Stolten, *J. Power Sources*, 326 (2016) 120.

326. K. E. Ayers, E. B. Anderson, C. B. Capuano, B. D. Carter, L. T. Dalton, G. Hanlon, J. Manco, and M. Niedzwiecki, *ECS Trans.*, 33 (2010) 3.
327. Q. Feng, X. Yuan, G. Liu, B. Wei, Z. Zhang, H. Li, and H. Wang, *J. Power Sources*, 366 (2017) 33.
328. D. S. Hall, C. Bock, and B. R. MacDougall, *J. Electrochem. Soc.*, 160 (2013) F235

© 2018 The Authors. Published by ESG (www.electrochemsci.org). This article is an open access article distributed under the terms and conditions of the Creative Commons Attribution license (<http://creativecommons.org/licenses/by/4.0/>).